



UNIVERSITATEA POLITEHNICA BUCUREȘTI
Facultatea de Științe Aplicate
Școala Doctorală de Științe Aplicate



Cristina-Antonia MARIN

STUDIES OF AIR POLLUTANTS THROUGH
EXPERIMENTAL TECHNIQUES AND MULTIFRACTAL
CORRELATION ANALYZES

REZUMAT

Doctoral committee

Prof Dr. Gheorghe CĂTA-DANIL	Universitatea Politeh- nica București	President
Prof Dr. Cristina STAN	Universitatea Politeh- nica București	Phd Supervisor
Prof Dr. Cristian FOCȘA	Universitatea Lile	Reviewer
Prof Dr. Mihail CRIS- TEA	Universitatea Politeh- nica București	Reviewer
CS I Bogdan ANTO- NESCU	Institutul Național de C-D pentru Optoelec- tronică INOE2000	Reviewer

București, 2022

Cuprins

1	Introduction	2
2	Evolution of gaseous atmospheric constituents in the cold season	3
3	The evolution of atmospheric particles in the cold season and the evaluation of their sources	7
4	Characterization of long-range transported aerosol using remote sensing and direct measurements	12
5	Measurement of secondary aerosols using the oxidation chamber	18
5.1	Evaluation of secondary aerosol in the oxidation chamber with the addition of SO ₂	19
5.2	Assessment of secondary aerosol in ambient measurement mode, without the addition of SO ₂	21
6	Multifractal correlation analysis	24
6.1	Cross-correlation between aerosol concentrations and weather data . .	24
6.2	Investigating Hurst Correlation Surfaces in Atmospheric Gases	26
6.2.1	Correlation between ozone and precursors	26
6.2.2	Cross-correlation between ozone, precursors and temperature .	27
6.3	Analysis of the correlation of time series with atmospheric parameters in two types of urban environments	29
7	Final Conclusions	31
8	List of contributions	41
8.1	Published Papers	41
8.1.1	ISI Papers	41
8.1.2	Additional ISI Papers	42
8.1.3	ISI indexed papers	42
8.2	International conference contributions	42

Introduction

Atmospheric constituents have been studied extensively lately because they affect the Earth's radiative budget and can **influence climate change**. Reports from the Intergovernmental Panel on Climate Change document these changes and show that various atmospheric compounds such as CO₂ and Black Carbon (BC) can have a warming effect, and SO₂ and organic carbon have a cooling effect (IPCC et al. (2021a,b)). Recent studies have shown that there is a link between air pollutants and various diseases such as infertility, premature birth, diabetes (Anderson et al., 2012; Gurjar et al., 2010). The size, concentration and composition of aerosols and gases are equally important in the impact on health. Due to current environmental issues, the complexity of atmospheric constituents, and the impact on human health, ongoing systematic studies are needed.

The purpose of the thesis is to contribute with new experimental studies and systematic analyzes to the characterization of polluting atmospheric constituents such as gases and aerosols, to the determination of their sources and origin, to investigate the formation of secondary aerosols under controlled conditions, as well as the identification of correlations between data-sets of pollutants and between them and the meteorological conditions.

The objectives pursued in the thesis are as follows:

- **O1** assessment of gaseous constituents and aerosols variation in the cold season
- **O2** estimation of contributing areas, local sources and long-distance transport for pollutants
- **O3** investigation of secondary aerosol formation using oxidation chamber as experimental technique
- **O4** multifractal nonlinear analysis of correlations between gases, aerosols and between them and meteorological parameters

The thesis is structured as follows: Chapter 1 presents experimental techniques and equipment used in the measurements and analyzes in this paper. Chapter 2 presents results of the variability of the concentrations of gaseous compounds (**O1**) and estimating possible contributing areas (**O2**). Chapter 3 includes particle concentration analysis (**O1**) and source estimation (**O2**). The following chapters investigate long-range transport / desert dust (**O2**) and secondary aerosols (**O3**). Because the characteristics of the compounds atmospheric and their sources are determined by complex dynamics, correlations between gas concentration data series, aerosol and meteorological parameters are approached by nonlinear analysis (**O4**) - Chapter 6.

Evolution of gaseous atmospheric constituents in the cold season

This chapter includes the variations analysis of gaseous constituents in a peri-urban area of Romania, results that were published in the journal *Atmosphere* (Marin et al., 2019b). The measurements were performed at Măgurele, a small residential town, located 10 km south of Bucharest, the capital city of Romania and about 2 km from Bucharest ring road. The gases measured during the campaign were: NO, NO₂, NO_x, O₃, SO₂, CH₄ and CO. In addition, the meteorological parameters (temperature, wind speed, wind direction, relative humidity, solar radiation and precipitation) were also analysed. The measurements were part of an international campaign.

Diurnal trend and chemical reactions between measured compounds

For the selected pollutants, the diurnal trends were calculated to highlight the local characteristics. Solar radiation is an important factor that influences the formation of O₃. The daytime trend of the solar radiation had a maximum value of 44W/m² at 11:00 UTC, and the average for the whole period was 10W/m². The highest concentration for O₃ (76 ppb) was recorded 2 hours after the maximum solar radiation value, 126W / m² on 1 March 2018 at 11:20 UTC. For the analyzed period, the concentrations NO and NO₂ were raised in the morning, during periods of heavy traffic, when a minimum concentration of O₃ was detected (Figure 2.1). Also, during the day, the concentration of NO decreased (reaching a minimum value around 13:00 UTC) as the radiation increased.

To highlight the sources, we used the non-parametric wind regression method (NWR) (Petit et al., 2017). The source for NO has been identified as being north from the measuring point, where the Bucharest ring road represents main contributing factor (Figure 2.1). NO₂ had a behavior similar to NO, but the concentration is more distributed in space, due to a longer residence time compared to NO and thus it could be transported over long distances before producing O₃.

The maximum value of solar radiation was recorded at the same time as the minimum concentration of NO₂ and the maximum concentration of O₃ was reached 1 hour after the maximum value of solar radiation was detected. Photochemical reactions are activated from 06:00 UTC, when the values of the solar radiation start to increase.

Weekly variation of NO, NO₂ and NO_x showed an upward trend during the working days, the maximum concentration being reached on Friday. Minimum concentration

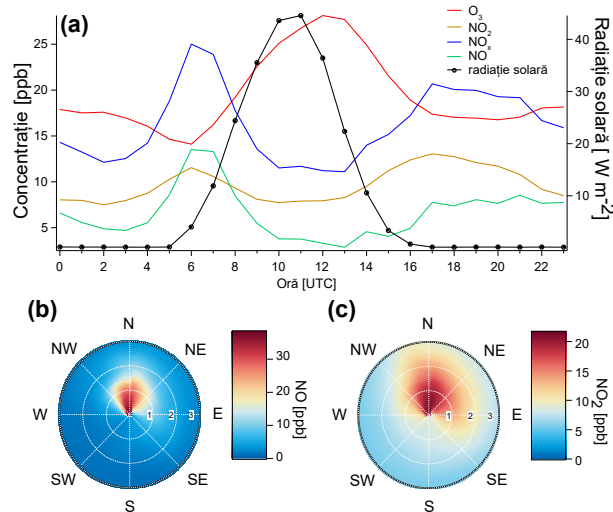


Figura 2.1: (a) Daytime trends for ozone (red line), nitrogen dioxide (orange line), nitric oxide (green line), nitrogen oxides (blue line) and solar radiation (black line), calculated for the cold season between 1 December 2017 and March 4, 2018. Source estimates for: (b) NO (ppb, colored by scale); and (c) NO₂ (ppb, colored by scale). For source estimation graphs, the inner white circles represent the wind speed in ms^{-1} . (Marin, C. A. et al., 2019b).

for NO_x has been recorded on Sunday, corresponding to the maximum concentration for O₃.

The sources for CH₄ and CO can be various and are associated with combustion processes. For the period discussed in this chapter, one of the main sources of CH₄ and CO was represented by the burning of fossil fuel (especially the source of traffic). The diurnal trends of CH₄ and CO showed similar trends to the diurnal variation of NO_x, with a higher concentration in the morning (05:00-06:00 UTC) and in the evening (around 19:00 UTC) (Figure 2.2). The CO daytime pattern showed a high value at 06:00 UTC of 0.42 ppm, but also a maximum (0.51 ppm), registered at 19:00 UTC. This behavior for CO can be explained by the diurnal evolution of the boundary layer (PBL) and the presence of two main sources, traffic and residential heating. The high concentration in the morning was more influenced by traffic, while in the evening the traffic contributed and also the residential heating. This explains why the maximum concentration of the second part of the day for CO was recorded at a different time than the maximum concentration observed in NO_x assigned to evening traffic.

These two sources for CO were also highlighted by the NWR model. By this method, a higher concentration in the north was estimated for CO, probably caused by traffic (as in the case of NO), but other sources are also highlighted, a smaller contribution in the area around the measuring point, probably produced by residential heating. For CH₄, the daytime analysis showed a higher concentration in the first part of the day, with a maximum in the morning, 2.72 ppm at 05:00 UTC. An increased concentration in the evening was also identified, with values of approx. 2.62 ppm in the period 19:00-20:00 UTC. This behavior with higher concentrations in the morning and evening is similar to the diurnal trend of NO_x, indicating a traffic source

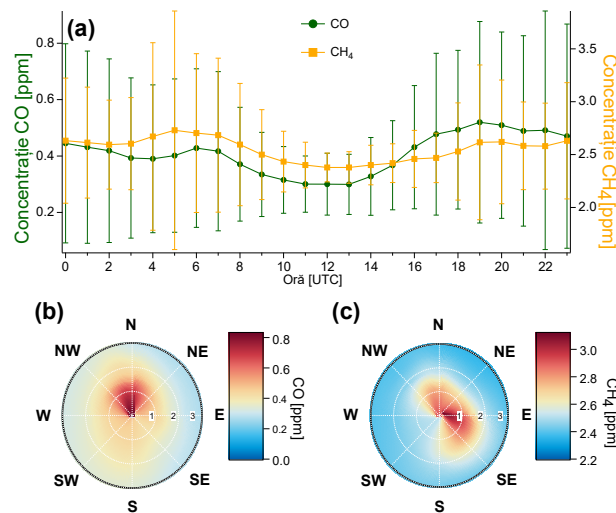


Figura 2.2: (a) Daytime trend calculated for the cold season between 1 December 2017 and 4 March 2018 for carbon monoxide (line green) and methane (yellow line), highlighting the peaks during the hours of morning and evening. Vertical error bars represent deviation standard from the average value. Source estimates are provided for: (b) CO; and (c) CH₄. For source estimation charts, white circles inland represents the wind speed in ms^{-1} . (Marin, C. A. et al., 2019b).

for CH₄. Source for CH₄ determined from NWR model (Figure 2.2), highlighted higher concentrations in the N and the SE, possibly due to traffic from the N and a landfill located 7 km from the place of measurement, in the SE direction.

Another atmospheric compound of interest in this study was SO₂, which can be emitted by burning biomass as a minor source, volcanic emissions and anthropogenic activities, such as burning fossil fuels. In addition, it can be formed by oxidation of other sulfur-containing gases produced in soil, plants, swamps and oceans due to phytoplankton activity. The diurnal trend of SO₂, which had a Gaussian form with a maximum value at noon, could not be explained by oxidation reactions with OH. Based on results from the literature (Adame et al., 2012) this daily variation has been attributed to long-range transport. The hypothesis has been validated, the NWR model illustrates higher concentrations in the V-SV part associated with wind speeds greater than 2 m/s, suggesting SO₂ transport from other regions.

Assessment of pollutant concentrations against European regulations

An important step in this study was comparison of measured values with the existing European limits, transposed into national law, for air pollutants. Limit values are set for an average of 1, 8 or 24 hours and in some cases this limit can only be exceeded by a limited number per year.

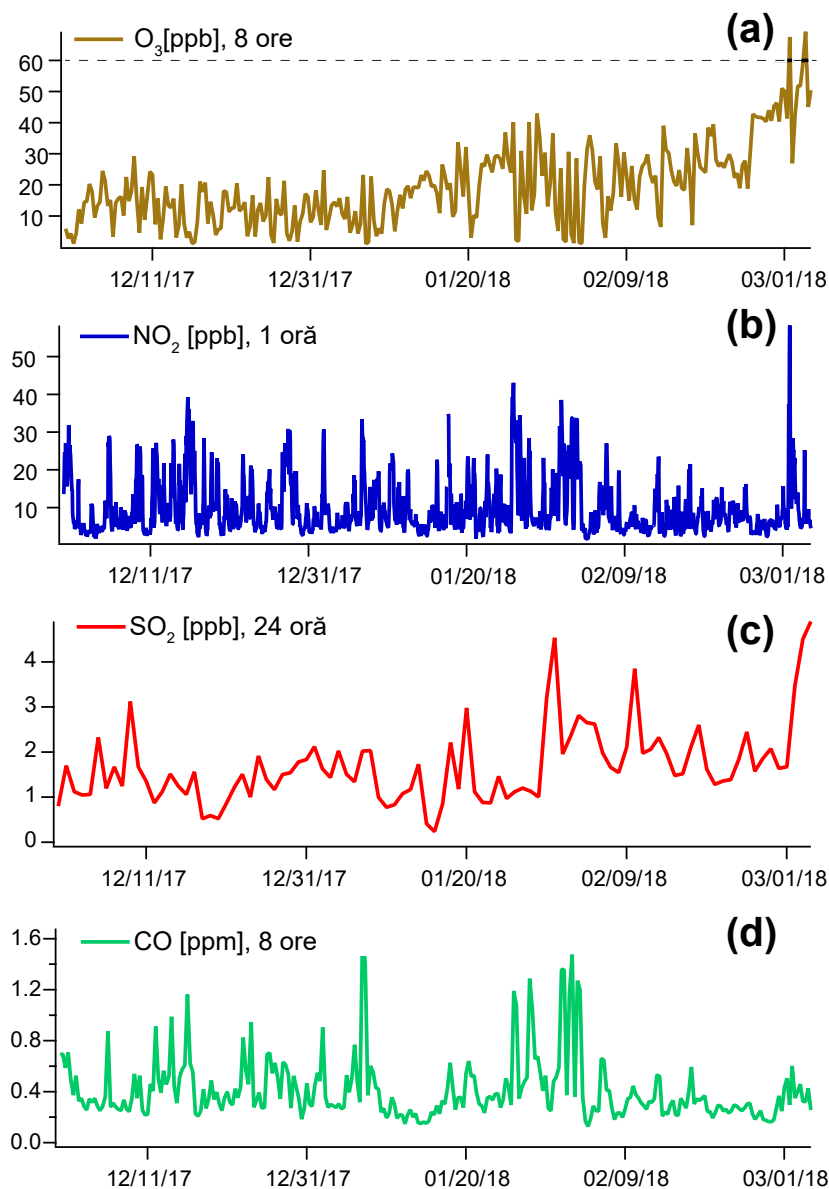


Figura 2.3: *Time series of pollutants calculated according to the mediation period specified in European Union legislation (indicated on each panel) for: (a) O_3 ; (b) NO_2 ; (c) SO_2 ; and (d) the concentration of CO . The horizontal line in (a) represents the limit value for O_3 in accordance with European Union law. (Marin, C. A. et al., 2019b).*

For these three-month measurements, only ozone exceeded the permitted average limit, having two values greater than 60 ppb on March 1 and March 3, 2018 and a value close to the limit, 59.3 ppb, also registered on March 3, 2018. The maximum hourly value for NO_2 , 58 ppb, was almost half of the limit, while the maximum average of CO was almost five times lower and the maximum value of SO_2 was ten times lower than the legal limit.

The evolution of atmospheric particles in the cold season and the evaluation of their sources

The analyzed period for aerosol measurements was the same as in Chapter 2, winter 2017/2018 (01 Dec 2017–03 March 2018). Data collected were: aerosol concentrations (PM_{10} , $PM_{2.5}$, PM_{10}) determined by the optical method; non-refractory aerosol concentrations PM_{10} (organic and inorganic fraction: NH_4 , NO_3 , SO_4) by mass spectrometry for aerosols, the concentration of carbon black aerosols obtained by an absorption technique. $PM_{2.5}$ particles were also collected on quartz filters and analyzed to determine the concentrations of elemental carbon, organic carbon, total carbon, levoglucosan and other sugars (arabitol, galactosane, mansan, glucose) in the fraction of $PM_{2.5}$.

The results of this study were presented at the European Aerosol Conference, 2019, Gothenburg (Marin, C. A. et al., 2019a; Marmureanu et al., 2019), and the methodology for determining the sources of organic aerosol is published, as a co-author in the paper (Mărmureanu et al., 2020).

Aerosol time variation

The measured concentrations were compared with the available air quality standards. $PM_{2.5}$ no daily limit is set by the European Standard, but the WHO recommendation for this is $25 \mu\text{g} / \text{m}^3$. Compared to these limits, in the 92 days of measurements, there were 28 exceedances for PM_{10} , and 72 days exceedances for $PM_{2.5}$, representing 78 % of the analyzed days. Compared to the new WHO limits set in September 2021 ($45 \mu\text{g} / \text{m}^3$ for PM_{10} and $15 \mu\text{g} / \text{m}^3$ for $PM_{2.5}$, daily averages), concentrations of PM_{10} was exceeded in 37 % of days, and concentrations of $PM_{2.5}$ were exceeded on all measurement days.

During the campaign, the total carbon concentration (TC) determined by the thermal method is $9.4 \mu\text{g} / \text{m}^3$, of which higher concentrations were detected for organic (OC) than for elemental carbon. OC accounted for 89 % of TC for the entire period. Higher EC values were recorded on December 16 ($5.9 \mu\text{g} / \text{m}^3$) and February 2 ($2.9 \mu\text{g} / \text{m}^3$), when high OC values were also detected ($17.8 \mu\text{g} / \text{m}^3$, respectively $20.6 \mu\text{g} / \text{m}^3$).

Source evaluation

Source apportionment was done using the PMF (positive matrix factorization) receptor-oriented method implemented in the SoFi software, Source Finder version 4.8. Data

obtained from aerosols mass spectrometry were used. The number of factors was chosen by running the model successively in several configurations, but the best solution, which could be explained physically and was validated by the comparison with external markers, is the one with four sources (factors). The spectral profiles determined for the four factors with the PMF model are illustrated in Figure 3.1.

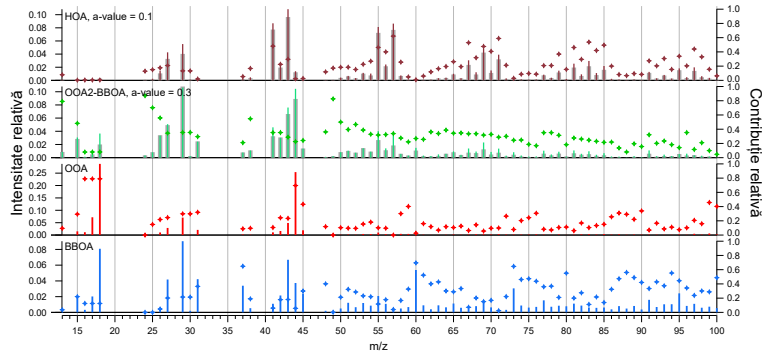


Figure 3.1: *Spectral profiles of determined sources*

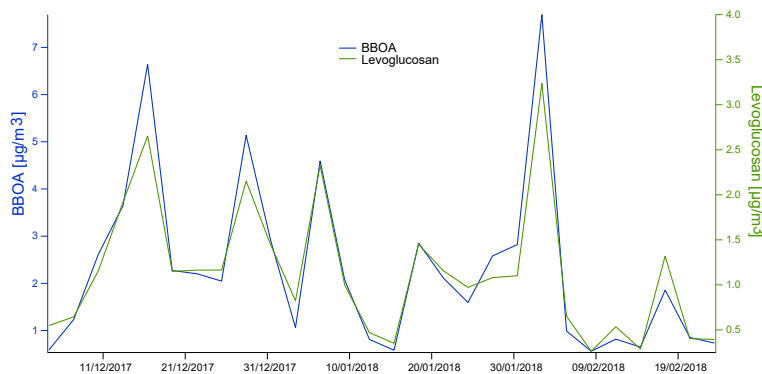


Figure 3.2: *Temporal variation of aerosol concentration from burning (BBOA, blue line) and levoglucosan concentration (green line)*

To validate the obtained factors, comparisons were made with external markers (BB_{ff} , BB_{wb} , NO_x , levoglucosan) and their diurnal trends were analyzed in comparison with the diurnal variations of the obtained factors. Acceptable correlations were obtained which helped to validate the determined factors. The R^2 between HOA - NO_x was 0.6; between OOA and NO_3 was 0.66, and between OOA₂- BBOA and BC_{wb} was 0.59. The BBOA profile was validated by comparison with BC_{wb} , $R^2 = 0.9$, and levoglucosan concentration values, $R^2 = 0.96$. The temporal variation of levoglucosan and BBOA (averaged at 24 hours and represented every third day according to levoglucosan measurements) is illustrated in Figure 3.2, where it can be seen that the same trend is observed for the two concentrations.

The characteristic spectra for each factor can be observed in Figure 3.1. HOA is generated from long chain saturated or unsaturated hydrocarbons and is characterized by the presence of peaks m/z 41 ($C_3H_5^+$), m/z 43 ($C_3H_7^+$), m/z 55 ($C_4H_7^+$),

m/z 57 ($C_4H_9^+$) (Crippa et al., 2014; Mărmureanu et al., 2020). The BBOA factor is confirmed by the presence of the increased signal at m/z 29 (CHO^+), 60 ($C_2H_4O_2^+$) and 73 ($C_3H_5O_2^+$) from levoglucosan fragmentation. The OOA factor is characterized by a large contribution of m/z 44 (CO_2^+). The factor OOA₂- BBOA (Crippa et al., 2013) is characterized by m/z specific for the two factors of which it is composed, BBOA and OOA, 44, 60, 73. Studies in Greece found a similar factor, corresponding to oxidized BBOA aerosol (derived from similar mass spectrometry data) detected throughout the year with certain seasonal characteristics (the factor contributed to the concentration of Org around 25 % in winter and 2-4 % in May-June) (Manousakas et al., 2020).

The average concentrations for the primary source factors are: 2.7 $\mu\text{g} / \text{m}^3$ for HOA, 2.7 for BBOA $\mu\text{g} / \text{m}^3$, and higher values were recorded for secondary sources: 3.7 $\mu\text{g} / \text{m}^3$ for OOA₂ –BBOA and 4.7 $\mu\text{g} / \text{m}^3$ for OOA. The majority of organic aerosol was allocated to secondary sources at 61 % and the remaining 39 % was allocated equally to primary sources. Of the secondary sources, OOA aerosol was the highest, accounting for 34.2 % of organic aerosol. A majority (55 %) of secondary aerosols was recorded for winter measurements in the same location for 2013 measurements (Mărmureanu et al., 2020).

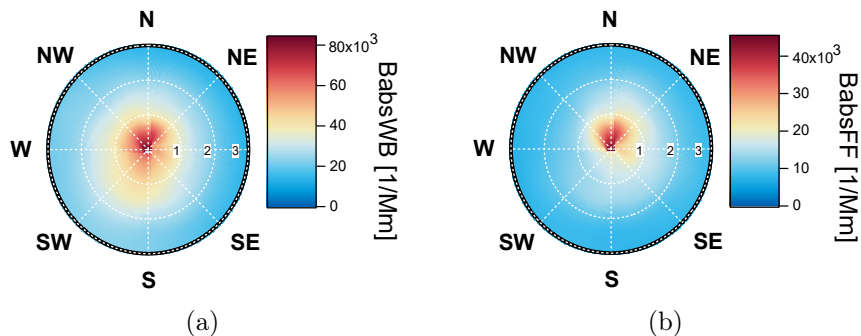


Figure 3.3: *Estimation of BC sources. The color code represents the absorption coefficient for aerosols resulting from biomass combustion (BabsWB) (a) and for those resulting from fossil fuel combustion (BabsFF) (b).*

Applying the NWR method, the main contributing areas can be estimated. The method was applied to the sources determined by the PMF technique for the organic spectra and for the BC sources. BC can be separated into two sources: BC resulting from fossil fuel combustion and biomass combustion. This is possible due to the differentiated absorption for the two sources in IR and UV, therefore different Ångstrom absorption coefficients are used for the two cases. The model highlights different spatial distributions for the two sources of carbon black. BC resulting from fossil fuel combustion is illustrated as the predominant source in the N part. This distribution is explained by the existence of the ring-road in the N part from the place of measurement, and does not indicate the use of fossil fuels (such as coal, fuel oil) in the residential area located in part E, S and V. The contribution of the carbon black source resulting from biomass combustion, specific to residential heating, is illustrated in Figure 3.3. It is observed that the measuring point is surrounded by a residential area. The distributions for these two sources are validated by the

distributions for NO_x and CO , as well as markers for traffic and residential heating, respectively (Chapter 2).

Diurnal Profiles

The diurnal variations of the investigated parameters are shown in Figure 3.4 with the corresponding error bars.

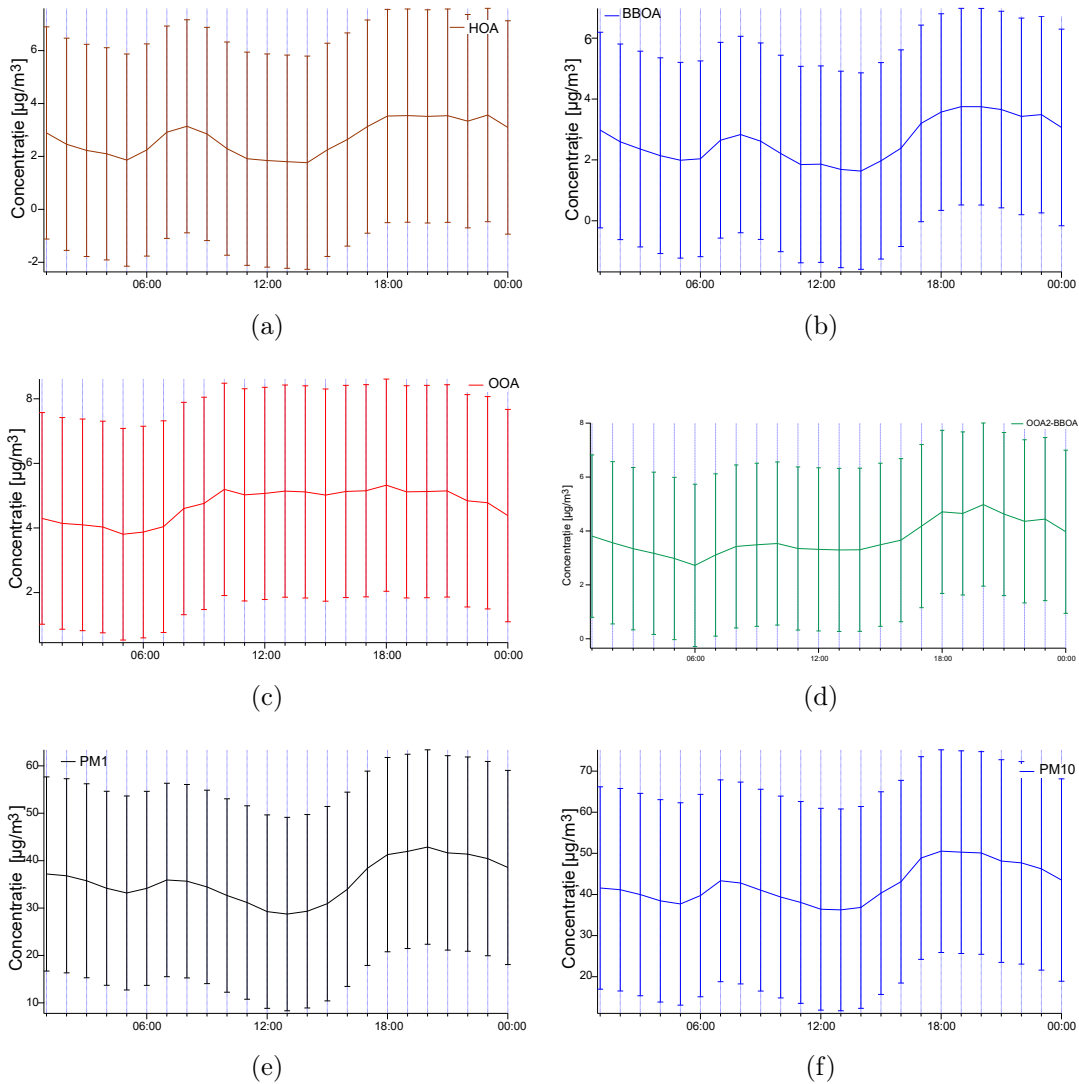


Figure 3.4: *Daytime variation and standard error bars for the parameters under investigation: (a) HOA, (b) BBOA, (c) OOA, (d) OOA₂- BBOA, (e) PM₁, (f) PM₁₀.*

The diurnal profiles of the primary factors show maximums with higher concentrations in the morning, around (local) time 08:00 and a plateau of higher concentrations in the afternoon (starting with 15:00 for the BBOA factor and with 18:00 for the factor HOA). These hours correspond to the hours for traffic, but also to the time at which residential heating usually takes place.

This variation, characterized by higher concentrations in the morning and evening and with lower values at noon, may also be influenced by the diurnal variation of

PBL. Unlike the specific traffic factor, HOA, the factor for aerosols resulting from residential heating, BBOA, has a peak around 12:00. Being a residential area, this can be explained by an additional heating of the houses at noon or the factor BBOA, derived by the PMF method, may also contain contributions from other sources. One possible factor is food preparation, COA. The COA factor is usually characterized by a diurnal profile with a higher concentration in the afternoon, around noon, and the spectral profile of this factor is identified by the presence of specific markers, m/z 55 and 57. For the COA factor the 55/57 ratio must be higher than the one calculated for the HOA factor. The ratio of m/z 55 to m/z 57 in HOA is 0.94 and in BBOA is higher, which indicates that the solution for BBOA is not completely separate and is a mixed profile between BBOA and COA. The separate, independent COA factor could not be extracted from the organic matrix by the PMF method, although in previous data this was possible (Mărmureanu et al., 2020). The diurnal profiles of the secondary sources have a different variation compared to the primary sources, their trend is flatter, characteristic of the secondary sources (Mărmureanu et al., 2020). The OOA factor is characterized by lower concentrations in the first part of the day, between 01:00 and 06:00, after which there is an increase in concentrations. The factor OOA₂- BBOA, has higher concentrations in the second part of the day, but also after 18:00, when higher concentrations for BBOA factor are observed.

The study aimed to evaluate the sources of aerosols and their characteristics in the cold season by using complex measurement techniques and methods of analysis. The data collected complied with the requirements of the EMEP / ACTRIS / CO LO SSAL campaign and was reported in International Database (EMEP). Experimental data collected using optical techniques (scattering, absorption) and mass spectrometry have been integrated into specialized studies on aerosol sources and composition in Eastern Europe. They were analyzed using the multi-linear regression method, implemented in the SoFi calculation program, to identify the generating sources. The composition and type of aerosols in PM_{2.5} were also determined to be in the majority ($\approx 90\%$) organic carbon and in lower percentages elemental carbon, and biogenic primary organic aerosol. Subsequent studies from the international campaign indicated that of the 25 measurement sites, the concentrations of elemental carbon in Magurele were the highest, and those of carbon black are in second place, the highest after Poland (Platt, 2019).

Characterization of long-range transported aerosol using remote sensing and direct measurements

This chapter presents a special Saharan dust intrusion event. The novelty of the study is given by the particularity of the event that took place between March 22-23, 2018, namely, the fact that the dust was deposited together with the snow. Because the dust was deposited in winter conditions, the snow had an orange color. This has raised concerns about the source of snow contamination. In this context, the importance of the investigations was due to the determination of the snow contamination and in particular to the determination of the source and type of aerosol. The results presented in this chapter were published as a co-author in the journal *Remote Sensing* (Mărmureanu et al., 2019).

Several types of data and tools were used in synergy to analyze this event: satellite data, forecast data for the dust aerosol optical depth(DOD), meteorological observations, in situ ground-based analysis, and also laboratory analyzes (chemical and imaging) for the dust snow sample.

Synoptic context

On March 21, 2018, at 12:00 UTC, a cyclone was formed in the Libyan area. During the early cyclogenetic processes, a significant amount of dust particles was lifted from the ground, so as highlighted in the satellite product. The transport of dust was further directed to the eastern Mediterranean and the Balkans: Greece, Bulgaria, southern Romania, Turkey, the Black Sea and southern Russia. Although visible in satellite images for the first 24 hours, the dust was covered in clouds during its transition. over the Balkans and the Black Sea.

According to satellite observations, the CAMS analysis (Figure 4.2) shows dust transport between 21:00 UTC on 22 March and 03:00 UTC on 23 March over Bucharest (i.e., the optical depth of the powder aerosol between 0.1 and 0.2) with a maximum dust advection over southeastern Romania (i.e., the optical depth of dust aerosol between 1.0 and 1.5).

Conditions before Saharan dust intrusion

From March 21 to 22, ground measurements for PM indicate decreasing values due to snow conditions. After the snowfall, the concentration of PM₁₀ reached 26.13 $\mu\text{g} / \text{m}^3$, and during the dust intrusion continued to decrease, reaching 18.04 $\mu\text{g} / \text{m}^3$ (Figure 4.3).

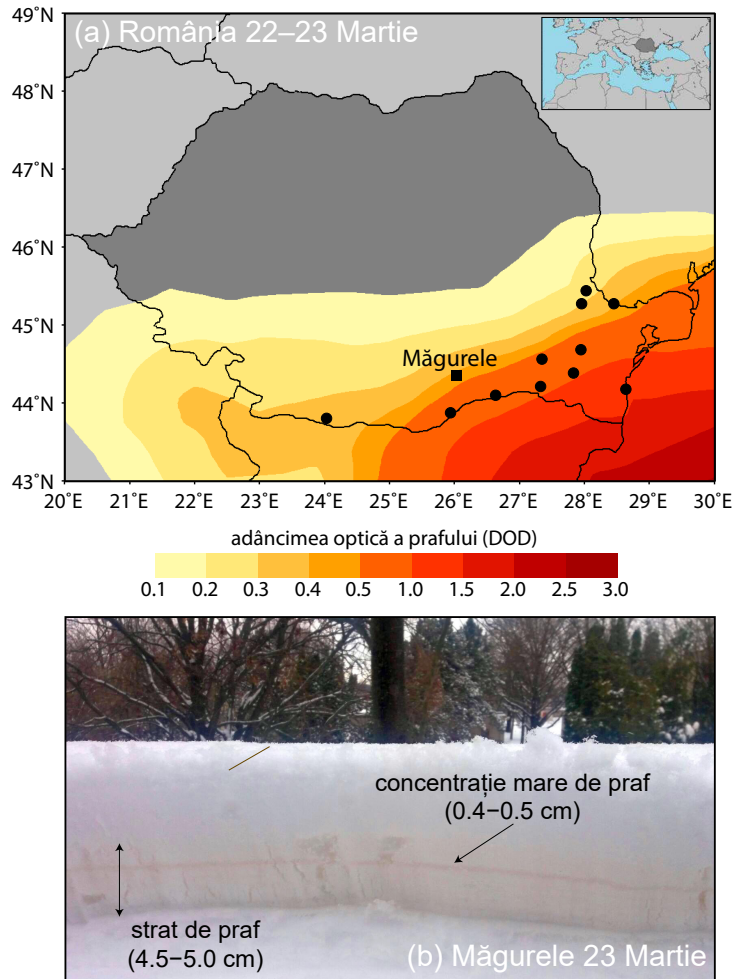


Figura 4.1: (a) Optical depth of dust aerosols over Romania, derived from data from the Copernicus Atmospheric Monitoring Service (CAMS), between 22 March 21:00 UTC - 23 March 06:00 UTC, coloured according to scale. The black circles are the places where there was a visual confirmation of the dust present on the ground. The black square represents the location of the Romanian Atmospheric 3D Observatory (RADO, Măgurele, Romania); (b) A section of the RADO snow layer showing the embedded dust layer (the thickness of the embedded dust layer is indicated together with the thickness of the high dust concentration layer). (Mărmureanu et al., 2019).

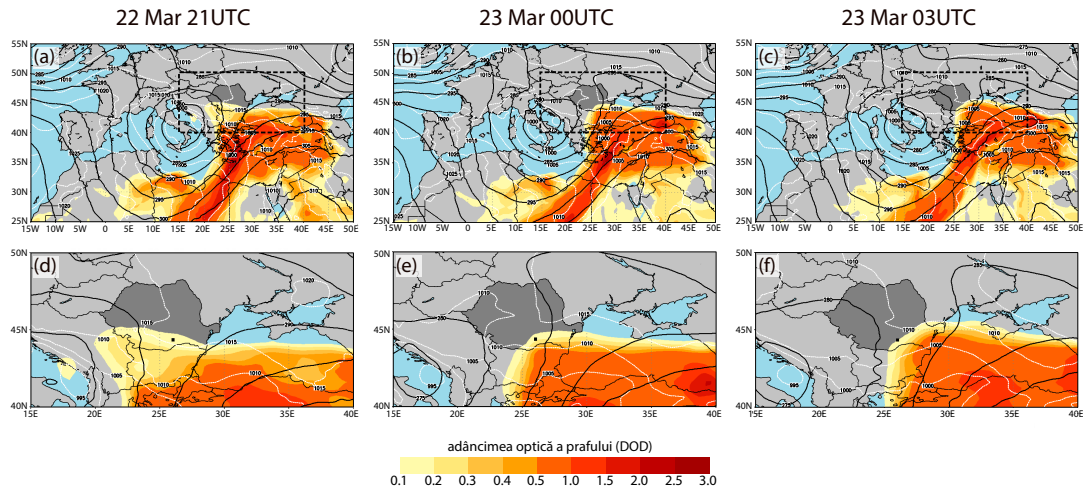


Figura 4.2: *Synoptic analysis based on ECMWF data for (a) 22 March 21:00 UTC; (b) 23 March 00:00 UTC; and (c) March 23, 03:00 UTC showing surface pressure (white contours, every 5 hPa), geopotential of 500 hPa (black contours) and optical depth of the powder aerosol resulting from CAMS (colored according to the scale bottom left). The regional scale analysis is presented in (d - f) for the area indicated by a dotted rectangle in (a - c). (Mărmureanu et al., 2019).*

Saharan dust in the snow

Because the snow started a few hours (i.e. 14:00 UTC on March 22) before the dust layer to appear above Romania (ie 21:00 UTC on March 22), was a clear stratification of the snow with layers of dust was observed. The largest layer dust concentration was 0.5 cm (Figure 4.1 b). The dust layer deposition was favored by the intensity of the snow. The snow increased from slightly continuous conditions starting with 18:00 UTC March 22, 2018 at continuous moderate snowfall at 00:00 UTC, March 23, 2018, followed by snow light continues at 01:00 UTC, which may explain the deposition of dust in a layer concentrated.

The sample collected from the snow was used to determine the chemical composition and morphology of particles in snow layers contaminated with Saharan dust. In general, Saharan dust is dominated by silicates (clay minerals, quartz) and, depending on its origin, carbonates (eg calcium carbonate). Previous studies (Telloli et al., 2018) used a number of markers (eg elementary ratio, diatoms) to identify the source of dust. The chemical composition of the sample, determined by the ICP-OES (Inductively Coupled Plasma-Optical Emission Spectrometry) method, was: Al 17.7 (± 6 %), Fe 15.9 (± 6 %), Ca 13.5 (± 5 %), K 4.1 (± 5 %), Mg 7.4 (± 5 %) and Na 2.3 (± 8 %) mg / l. Elemental ratio were used, according to Scheuven et al. (2013), to characterize the origin of the particles. For the analyzed sample, the ratio $(Ca + Mg) / Fe$ was 1.39 indicating a source located in Algeria, Libya or Egypt. Lower values (i.e. 1.2 ratio) were reported for the belt sub-Saharan belt (Scheuven et al., 2013). Lafon et al. (2006) used as indicator Ca for dust source, with large amounts of Ca indicating a North African origin.

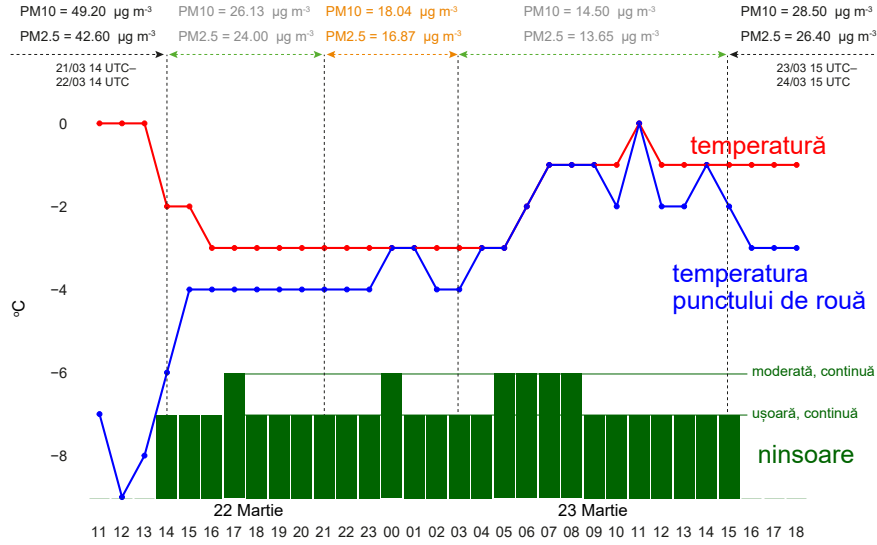


Figura 4.3: Temperature variations (red line) and dew point temperature (blue line) between March 22-23, according to the recording from the Filaret weather station (Bucharest). The concentration of PM_{10} and $PM_{2.5}$ is indicated at the top for the period before the snow starts (black, March 21 14:00 UTC - March 22 14:00 UTC), during the snow, but before dust intrusion (gray, March 22 14:00 UTC - 21:00 UTC), during the snow and dust intrusion episode (orange, March 22 21:00 UTC - March 23 03:00 UTC), during the event of snow, but after the intrusion of dust over Bucharest (gray, March 23 03:00 UTC - 15:00 UTC) and after the snow stopped (black, March 23 15:00 UTC - March 24 15:00 UTC). (Mărmureanu et al., 2019).

The SEM / EDX analysis also indicated that dust particles collected from melted snow is dominated by crystalline morphologies (e.g. rhombohedral and scalenohedral) (Figure 4.4), angular and spherical Fe particles for example, hematite - Fe_2O_3 , goethite - $FeO-OH$), simple or in combination with clay minerals. Ti particles were found in combination with others elements (i.e. TiO_2) as part of conglomerate structures (Figure 4.5).

The optical properties of the aerosols were also determined from the snow sample. The Ångström scattering exponent (SAE), derived from direct measurements, at 450/700 nm wavelengths, of re-suspended dust particles is $0.93 (\pm 0.03)$ - characteristic for transported dust (Hallar et al., 2015). SAE values of 0.5 are specific for dust near sources (Müller et al., 2010) and values around 1.3 for urban sites (Ealo et al., 2016). For the sample we analyzed, it was very likely that the dust was contaminated with marine and anthropogenic aerosols during transport across the Mediterranean Sea and southern Europe, which influenced the optical properties. The SAE values registered in Romania are similar to those reported for the Iberian Peninsula (Ealo et al., 2016). Previous studies have shown that during dust intrusion episodes the SAE decreases, while the Ångström absorption ratio (AAE) increases (Ealo et al., 2016). This was also observed for the dust analyzed in this case, as the AAE was 1.95 for 450/700 nm.

The single scattering albedo (SSA) was calculated for each nephelometer wavelength. SSA values ranged from 0.84 at 450 nm to 0.89 at 700 nm. The previously reported

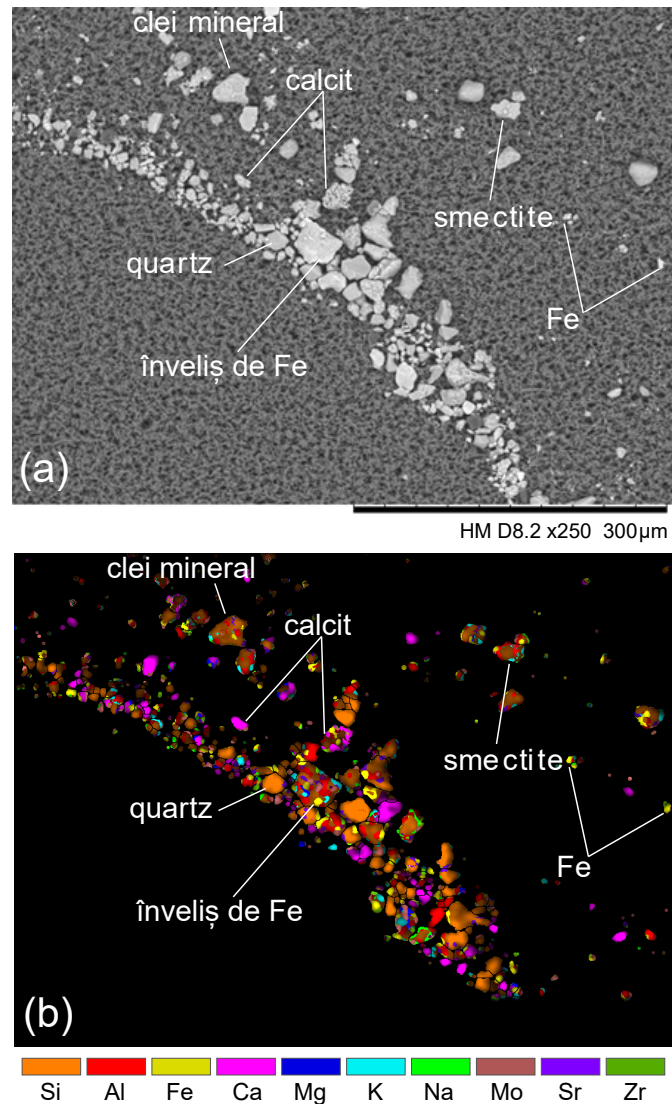


Figura 4.4: Saharan dust deposited on the carbon filter viewed using (a) scanning electron microscope; and (b) Energy-dispersive X-ray spectroscopy. In (b) the image was obtained using all the pixel value maps. Based on the elemental composition, the presence of particles rich in calcite, quartz and Fe was highlighted. (Mărmureanu et al., 2019).

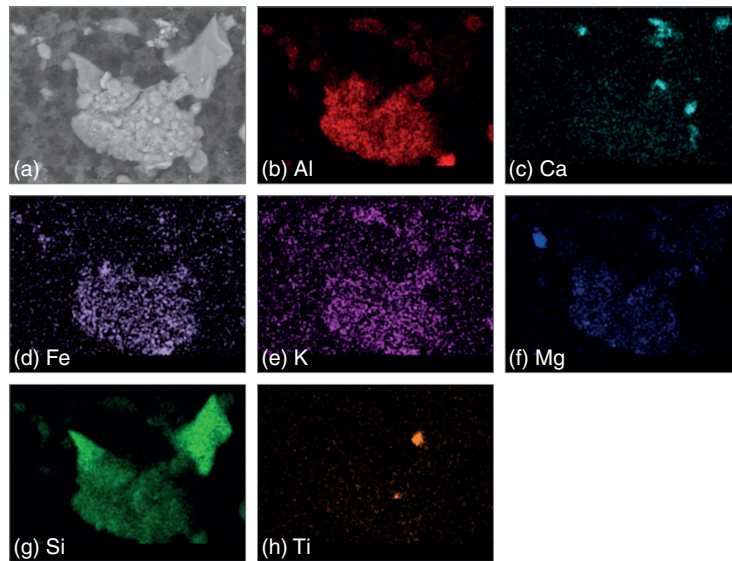


Figura 4.5: *SEM / EDX images of the conglomerate. (a) SEM image, (b - h) elementary composition derived from EDX for Al, Ca, Fe, K, Mg, Si, Ti.* (Mărmureanu et al., 2019).

SSA values (Moosmüller et al., 2012) were anti-correlated with Fe content, low values for SSA (i.e. 0.86 at 405 nm) are characteristic for dust with a high Fe content (ie 30 %). In our sample, the SSA was 0.84–0.89 corresponding to the Fe content of 15.9 mg/l.

The asymmetry parameter (g) is used in radiative transfer models, so it is important in Saharan dust intrusion events. For the sample analyzed in this study, g measured at 550 nm (Andrews et al., 2006) had a value of 0.604, which is also similar to the values previously reported for the sites in the Iberian Peninsula (Ealo et al., 2016). Other in situ measurements for Saharan dust events showed that g can be between 0.5 and 0.75 (Ogren et al., 2006). Values from 0.81 ± 0.008 to 0.92 ± 0.004 for SSA and between 0.61-0.069 for g were reported in Italy during a Saharan dust event in North Africa (Donateo et al., 2018).

This chapter presents a study for the characteristics of long-range aerosols. The analysis was possible due to a Saharan dust intrusion event, which had a major impact on southern Europe. The detection of the type of aerosol was made in this study by taking samples from the snow deposited at ground. Dust snow samples were analyzed by complementary experimental techniques: optical, SEM-EDX imaging, optical and ICP-OES emission spectrometry.

Measurement of secondary aerosols using the oxidation chamber

The secondary organic aerosol, SOA, are the major component (50–85 %) of the organic aerosol (Jimenez et al., 2009). Also it was shown that SOA represents the major fraction of aerosol at the analyzed site, Magurele (Chapter 3). Because its formation is not fully understood, we conducted studies on the generation of SOA from ambient conditions using an oxidation chamber.

The reactor used is the Potential Aerosol Mass Flow Reactor (PAM) which consists of a cylinder with a total volume of 13.3 l. It has four mercury lamps which help to form an oxidizing medium (OH radicals) for the generation of SOA. To evaluate the properties of the formed aerosols, the camera is connected with instruments for determining the mass concentration (ACSM-mass spectrometry for aerosols) and numerical concentration (SMPS- for detecting submicron particles), gas analyzers (O_3 , SO_2). The experimental setup is illustrated in Figure 5.1.

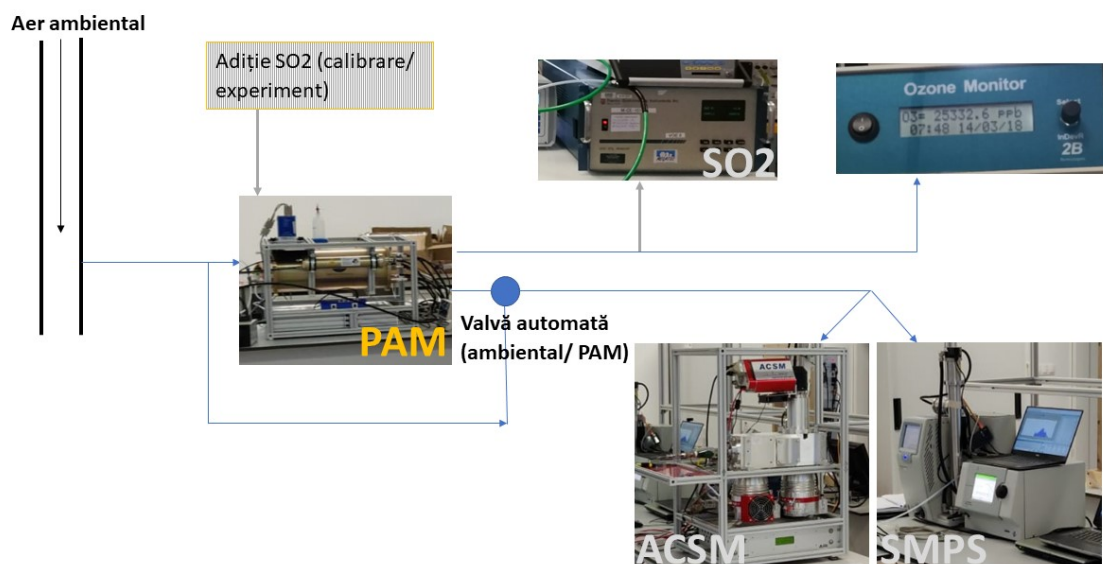


Figura 5.1: *Experimental set-up*

The formation of the secondary aerosol from the ambient aerosol was investigated in this chapter. The analysis of the two types of aerosol was done using an automatic valve that allows instruments to collect air from the outdoor or from the reaction

chamber. The aerosols measured from the outdoor were considered to be primary, and the concentrations (numerical and mass) for the secondary ones were calculated as the differences between the the concentration from the reaction chamber and the primary aerosols. For the SOA study using the reaction chamber, several measurement set-ups were used. These involved changing the voltage on the lamps in several steps to create a more or less oxidizing environment. The oxidation power in the chamber can be determined by calibration. Using known SO_2 concentrations for different measurement sequences we determined the OH concentration and oxidation time. If the primary aerosol analyzed had low concentrations, sulfur dioxide was used to initiate the process of generating the secondary aerosol.

5.1 Evaluation of secondary aerosol in the oxidation chamber with the addition of SO_2

A first case study included the evaluation of secondary aerosol by adding sulfur dioxide to the oxidation chamber. The gas was introduced with a constant concentration and flow. Figures 5.2 - 5.3 show the dimensional distributions of the primary and secondary particles, respectively. The differences between the two types of aerosols are observed: the primary ones have dimensions between 30 and 200 nm, while the secondary aerosol is formed up to the size of 90 nm.

The concentrations of the secondary particles reach values up to $14000 \text{ \#} / \text{cm}^3$. The primary aerosols are not constant over time, an intrusion is observed in the second half of the day, starting at 18:00 (Figure 5.2). Figure 5.3 shows that the value of the numerical concentration of the particles is not strongly dependent on the applied voltage. The values of the number of particles do not vary much for a cycle of lamp voltages.

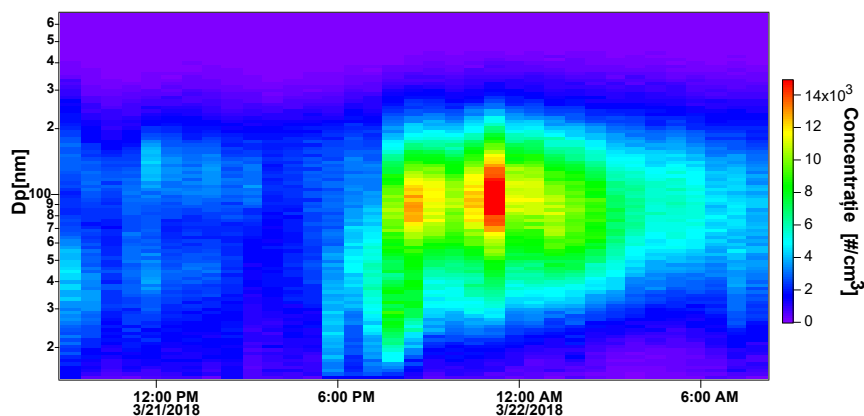


Figure 5.2: *Temporal variation of the dimensional distribution of the primary particles for the experiment with the addition of SO_2 . The color code represents the numerical concentration of the particles. Only environmental measurements are shown.*

For the primary organic and nitrate aerosol, an increase of the concentration is observed in the second part of the day, which is in accordance with the numerical concentration of the primary aerosol (Figure 5.2). The mass concentrations of the secondary aerosol are shown in Figure 5.4. The concentration of the secondary aerosol

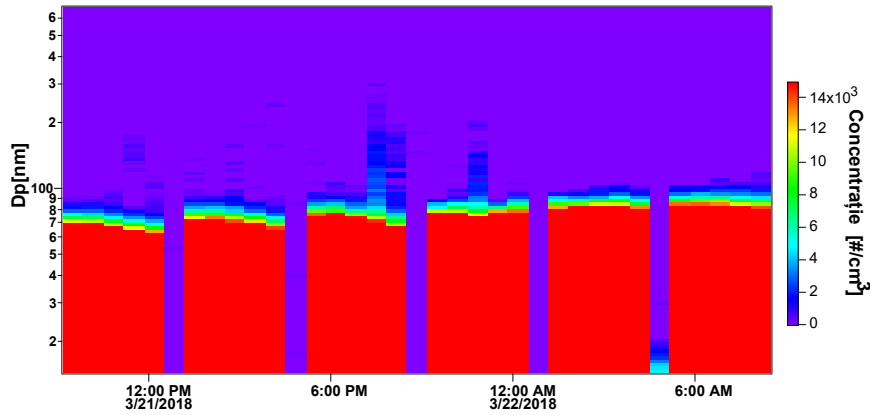


Figure 5.3: *Temporal variation of the dimensional distribution of the secondary particles for the experiment with the addition of SO_2 . The color code represents the numerical concentration of the particles. Only measurements corresponding to secondary particles are shown.*

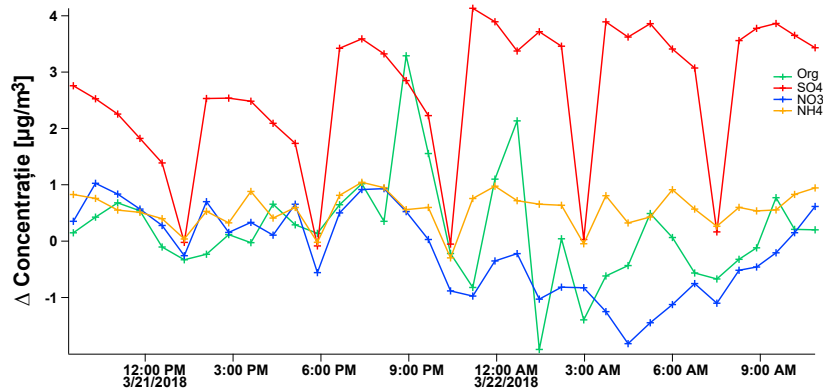


Figure 5.4: *Temporal variation of the mass concentration of secondary particles: organic aerosols (green line), nitrate (blue), sulfate (red); ammonium (orange) for the experiment with the addition of SO_2 . Only secondary particle measurements are shown.*

does not show high values, the maximum reached being $4 \mu\text{g}/\text{m}^3$ for the sulfate type aerosol.

Figure 5.4 shows the cyclic behavior of the sulphate concentration as a function of the six voltages applied: 3, 2.8, 2.3, 2, 1.8 and 0 V. Secondary organic aerosol, nitrate and ammonium do not have a cyclic structure, and their values decrease during the experiment, which indicates the volatilization under these experimental conditions.

5.2 Assessment of secondary aerosol in ambient measurement mode, without the addition of SO₂

SOA measurements in the Magurele area - winter

The measurements were made in Măgurele, between December 2020 and January 2021. This season was chosen because usually the concentrations are higher and there are several primary sources (Mărmureanu et al., 2020). The ozone monitor, SMPS and ACSM were used to investigate the formation of aerosols in the reaction chamber. To create an oxidizing environment the voltage applied to the lamps were between 1.5, 2 and 3 V.

The temporal evolution of the dimensional distribution of aerosols highlights the presence of aerosols up to 100 nm and higher concentrations for aerosols up to 60 nm, corresponding to the cycles of variation of lamp voltages. In the numerical concentrations only two stages of particle formation corresponding to voltages of 2 and 3 V can be observed. For the voltage of 1.5 V no significant increase of particles with a diameter of less than 60 nm is observed, and the numerical particle concentrations corresponding to this voltage are similar to the concentrations obtained when the lamp voltage is 0 V.

Figure 5.5 shows the temporal variation of the secondary aerosols obtained for the 2 V voltage (defined as the difference between the measurements corresponding to the 2 V cycles and the 0 V cycles).

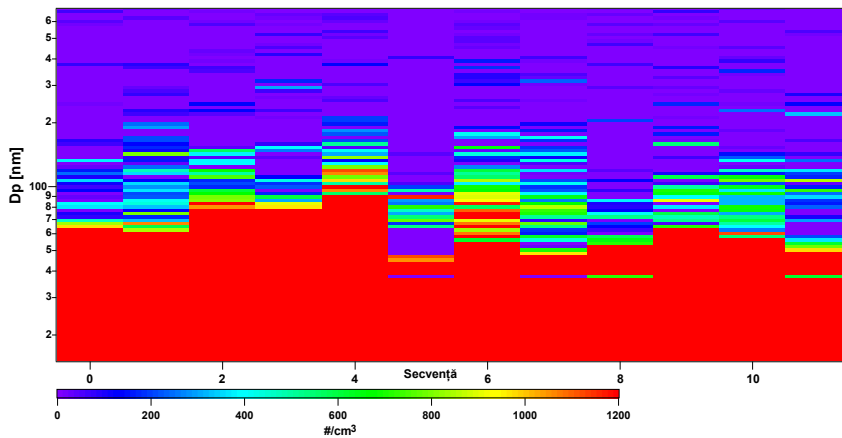


Figura 5.5: *The temporal variation of the dimensional distribution of the secondary particles obtained at a lamp voltage of 2 V, for the experiment in ambient regime, in the cold season. The color code represents the numerical concentration of the particles. This graph shows only the measurements corresponding to the secondary particles, being defined as the difference between the particles measured in the reaction chamber and the ambient ones.*

For 1.5 V measurements, concentrations around 800 #/cm³ are observed for aerosol size between 20 and 200 nm, but not for all measurement sequences. We can conclude that for this voltage the ideal conditions for the generation of secondary aerosols are not formed, but certain increases of concentrations are observed. For measurements performed when the lamp voltage is set to 2 V, high concentrations (over 1200 #/cm³) are observed for aerosols up to 70 nm, but also for particles

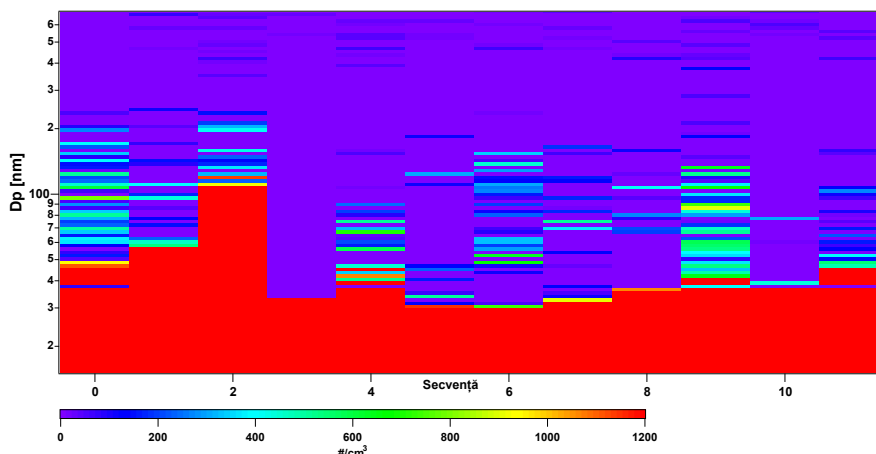


Figura 5.6: *Temporal variation of the dimensional distribution of the secondary particles obtained at a lamp voltage of 3 V, for the experiment in ambient regime, in the cold season. The color code represents the numerical concentration of the particles. This graph shows only the measurements corresponding to the secondary particles, being defined as the difference between the particles measured in the reaction chamber and the ambient ones.*

up to 200 nm (Figure 5.5). For the 3 V measurements, it is found that the size of the particles formed is smaller (on average about 40 nm) compared to the measurements corresponding to the 2V. For ambient aerosols, the highest concentration is for organic aerosol, followed by sulfate. The average concentration of the primary particles was $4.74\mu\text{g}/\text{m}^3$, of which 48 % was represented by Org and 23.7 % SO_4 . NO_3 and NH_4 had similar percentages, 15.7 % and 11.6 %, respectively. Chlorides accounted for only 1 % of the minority. The highest concentrations were recorded for Org, $14.88\mu\text{g}/\text{m}^3$ on 15.01.2021,07:51 UTC, respectively $14.36\mu\text{g}/\text{m}^3$, at the beginning of the experiment, on 14.01.2021,15:31 UTC. The concentrations detected in the experiment are lower than those usually recorded during the cold season (Chapter 3).

The variation of the organic compounds resulting from the oxidation chamber as a function of the voltage applied to the lamps is shown in Figure 5.7.

For the secondary particles, the detected concentration is higher than $0\mu\text{g}/\text{m}^3$, which indicates an increase of the concentrations in the oxidation chamber, compared to the environmental measurements. Only a quarter of the points have values less than $0\mu\text{g}/\text{m}^3$. The highest concentration ($5.3\mu\text{g}/\text{m}^3$) was obtained for two points, when the lamp voltage was 2V. The concentration corresponding to the 3 V measurements are generally (10 points out of 12) lower than in the case measured for 2 V. The decrease of the concentration at a higher voltage indicates a possible fragmentation of the particles generated in the oxidation chamber. Aerosol fragmentation cannot be ruled out for 2V voltage, as there is not possible to differentiate between fragmentation and particle formation, but most likely, at this stage, a fragmentation is possible, but it is accompanied by particle formation and/ or growth. Also, the evaporation of particles at the values used for lamp voltages is possible.

The generation of the sulphate secondary aerosol is shown in Figure 5.8. For this case, the concentrations are lower and fewer points are positive (39 % of points are negative). The highest concentrations are about $2.2\mu\text{g}/\text{m}^3$, recorded for 2 points

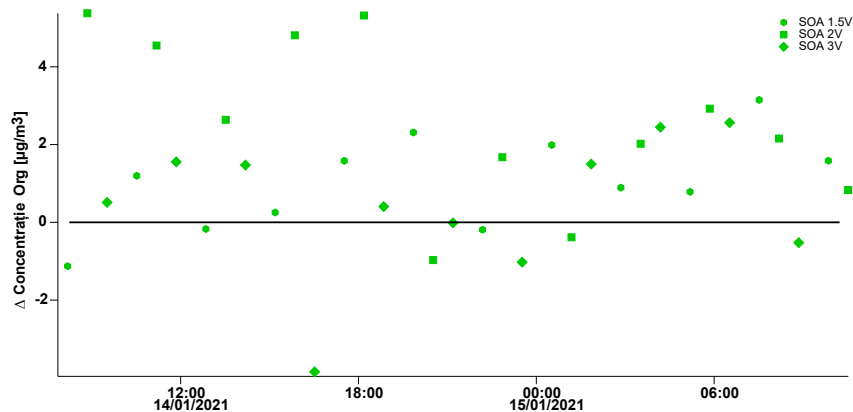


Figure 5.7: *Temporal variation of the mass concentration of the secondary organic aerosol for the experiment in the ambient regime, in the cold season. The hexagonal point indicates the measurements at 1.5 V, the square at 2 V, and the rhombus at 3 V.*

measured in 2 V mode and one point measured in 3 V mode. In this case, higher concentrations are also observed for 2 V measurements.

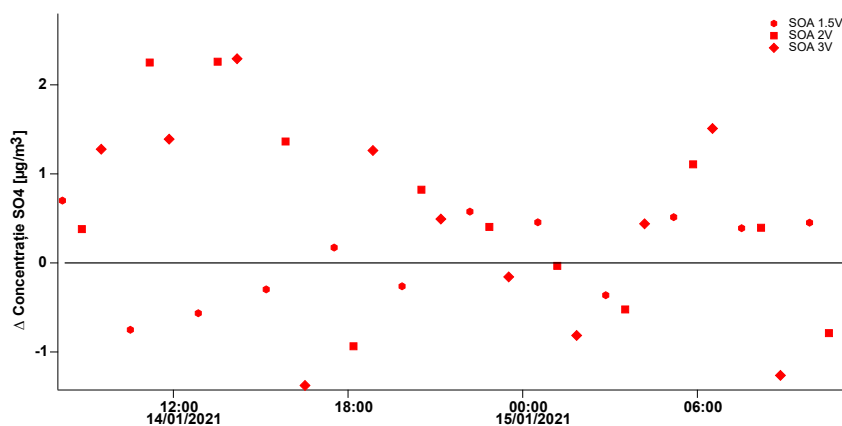


Figure 5.8: *Temporal variation of the mass concentration of the secondary sulphate aerosol for the experiment in the environmental regime, in the cold season. The hexagonal point indicates the measurements at 1.5 V, the square at 2 V, and the rhombus at 3 V.*

For the ammonium and nitrate aerosols generated in the oxidation chamber no significant increases are observed, the obtained concentrations are lower than $1.5 \mu\text{g}/\text{m}^3$. The explanation can be the fact that these two species are not very stable, and under the conditions obtained in the oxidation chamber, they can volatilize. Other studies in the scientific literature have investigated the increase in the mass or numerical concentration of aerosols during environmental measurements coupled with the PAM. The measurements in Sweden were the first experiments in Europe, and the measurement campaign lasted 2 months (Ahlberg et al., 2019). A net loss of 10 % particle concentration was observed, correlated with the temperature in the oxidation chamber and the exposure to the OH radical. The loss of particles has been attributed, as in the case of the experiment presented in this chapter, to the fragmentation and evaporation reactions caused by the difference in temperature between the oxidation chamber and the environment.

Multifractal correlation analysis

The classical correlation methods are valid for stationary data series, for which the statistical properties do not change over time and the samples with the same number of points have the same statistical distribution. For non-stationary data series, which are representative of the atmospheric system, the intrinsic characteristic is the non-linearity, and for the data set non-linear analyzes are needed. Some of these methods are based on the concept of fractal. The first algorithms used modeled the data series as monofractal - described by a single scaling exponent, with the same properties at different scales of analysis, then multifractal models have been developed, applicable to complex and heterogeneous systems, characterized by several characteristic exponents.

This chapter contains results of multifractal cross-correlation analyzes using generalized Hurst exponents (in the representation of curves or surfaces) for atmospheric data such as gases or aerosols concentrations and between them and some meteorological parameters. The presented results are based on the papers published in Romanian Journal of Physics **Marin, C.** et al. (2018), in Scientific Physica A: Statistical Mechanics and its Applications Stan et al. (2020) and in Bulletin Series A: Applied Mathematics and Physics **Marin, C.A.** et al. (2021).

6.1 Cross-correlation between aerosol concentrations and weather data

The data used in this study were collected in a measurement campaign conducted in Magurele, between July and August 2016. The meteorological data were measured simultaneously with the aerosol data, with a resolution of 15 minutes. For aerosols, numerical concentration ($\# / \text{cm}^3$) and average radius data, measured with a particle analyzer: APS (Pfeifer et al., 2016), were used. The chosen meteorological parameters were: air temperature (Temp), wind speed (WS), solar radiation (SolRa), relative humidity (HUM) and pressure (Pres).

Figure 6.1 illustrates the corresponding singularity spectrum $f(\alpha)$. The shape and distribution of the curves give information about the characteristics of aerosol data and their associated structures. The aerosol concentration curve has the largest range in terms of fluctuations and singularity, larger than the average radius. The left branch of the multifractal spectrum $f(\alpha)$ corresponds to the positive values of q and describes the area of large fluctuations in concentration or radius. It is visibly smaller than the branch on the right that corresponds to the negative values of q . This assumes that the range of fractal dimensions for large fluctuations is smaller than that corresponding to small fluctuations, which can be explained by probably

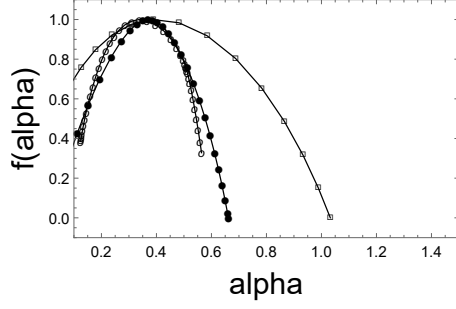


Figure 6.1: *Multifractal spectra for aerosol concentration series (squares), mean radius (empty circles) and correlated data series (balls)*(Marin, C. et al., 2018).

the occurrence of some aggregates.

Theoretically, low values of $f(\alpha)$ characterize a rare occurrence of isolated high values in a data sample, while higher values of $f(\alpha)$ are typical for a higher occurrence frequency and density of small numerical values. Similar to the situation of theoretical multifractal curves, for most of the singularity exponent interval, the curve for the cross-correlation spectrum (solid circles in Figure 6.1) is located between the curves corresponding to the singularity spectra of the two independent data sets.

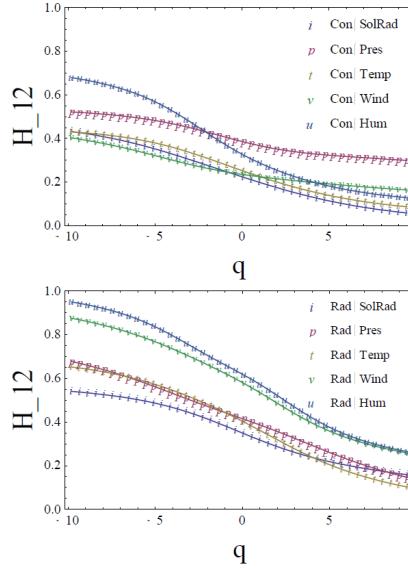


Figure 6.2: *Generalized Hurst exponents for the cross-correlation between total concentration and meteorological parameters (top panel) and between mean radius and meteorological parameters (bottom panel)*(Marin, C. et al., 2018).

The figure 6.2 shows the generalized Hurst exponents ($H_{12}(q)$) for the cross-correlation between: total concentration and meteorological parameters (top panel) and between average radius and meteorological parameters (bottom panel). The curves for different parameters are made explicit in each figure. It is observed that Hurst exponents for the cross-correlation of the mean radius with the meteorological parameters show lower values compared to those of the total concentration. The curves in Figure 6.2 are fitted with logistic functions (Stan et al., 2017).

From the values of H_{12} for $q = 2$ it is observed that all pairs have values less than 0.5, which means anti-persistence, except for the cross-correlation radius - humidity (Hum) which is higher of 0.5. In this case, the correlation for the pair is persistent, which means that any increase/decrease of the values in one series is more likely to be followed by a new increase / decrease in the values of the other series.

This study clearly demonstrates the correlation between weather parameters and the total particle concentration and the particle diameter.

6.2 Investigating Hurst Correlation Surfaces in Atmospheric Gases

A more detailed analysis of the cross-correlations between meteorological parameters and measurements of gaseous air pollutants at different time scales is performed using representations of the surfaces of the generalized Hurst exponents.

6.2.1 Correlation between ozone and precursors

After standardizing the data, the first step in the analysis was to construct the graphs of the fluctuation functions and then the dependence of the generalized Hurst exponents on the order of the fluctuation q , for different time scales s .

All individual Hurst surfaces for NO_x , THC, NMHC, and CH_4 were found to have multifractal characteristics. We made a quantitative distinction between the characteristics of these data sets by calculating two parameters defined in our study: the strength of multifractality and the variation of cross-correlation.

$$\Delta_s H(q) = |H(q_{max}, s) - H(q_{min}, s)| \quad (6.1)$$

$$\Delta_q H(s) = |H(q, s_{max}) - H(q, s_{min})|. \quad (6.2)$$

These coefficients provide clear and relevant information on the properties of each individual series, but also on the interdependencies in the correlated data series.

For O_3 , NO_x and THC changing the parameters between the argument limit values is similar, showing a decrease when s and respectively q increase. However, while the difference is large for O_3 , the variation is much smaller for the other two compounds. This is explained by the fact that ozone has the highest degree of variability, due to the existence of a large number of variables that affect its dynamics (Sillman, 1999). A different situation is observed for the case CH_4 and NMHC. Both parameters show an increase, while the respective arguments increase, with a greater difference observed in the case of CH_4 .

Hurst exponent values for small and large fluctuations show a strong persistent cross-correlation for each data pair O_3 and precursors. In the case of the cross-correlation calculation described by the values in Table 6.1, it is found that both the strength of multifractality and variation of cross-correlation increase with the increase of s and q , respectively. Similar to the situation for individual data, for each combination, the variation of the two parameters between the limit values of those arguments is the same within the accuracy limits of the calculation.

Table 6.1: The strength of multifractality and the variation of cross-correlation for the investigated pollutants

	$\Delta_s H(q)$		$\Delta_q H(s)$	
	s_{min}	s_{max}	q_{min}	q_{max}
O ₃ – THC	0.31	0.61	0.33	0.63
O ₃ – NO _x	0.46	0.69	0.40	0.62
O ₃ – CH ₄	0.25	0.67	0.21	0.63
O ₃ – NMHC	0.31	0.66	0.23	0.59

6.2.2 Cross-correlation between ozone, precursors and temperature

Figure 6.3 shows the areas $H_{XY}(q, s)$ for the cross-correlation between O₃, NO_x, THC, NMHC, CH₄ and temperature. The same complex, multifractal patterns are observed, depending on the time scale. However, the surfaces of the Hurst exponents of each temperature-pollutant compound have different characteristics in the small and large scale ranges.

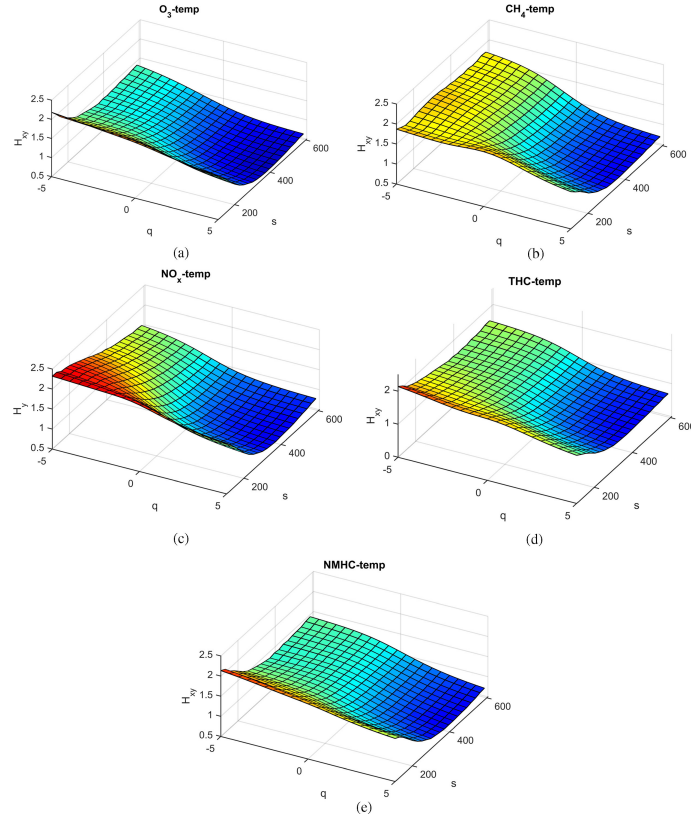


Figure 6.3: Generalized Hurst surfaces for cross-correlations between air pollutants and temperature (Stan et al., 2020).

The analytical fit of the curves generating $H_{XY}(q, s)$, proposed in the study is:

$$H_{XY}(q, s) = n_s + \frac{d_s}{1 + e^{g_s(q-f_s)}}, \quad (6.3)$$

where n_s is the minimum point of the curve, d_s is the maximum point, g_s is a parameter that represents how steep the function is and f_s is the point middle of the sigmoid (Stan et al., 2017). The coefficients n_s , d_s , g_s and f_s depend on the specific scale s .

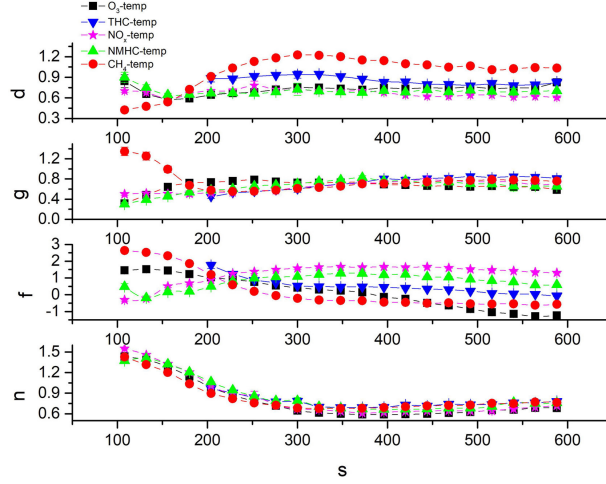


Figure 6.4: Values of fitting parameters for cross-correlations between air pollutants and temperature (Stan et al., 2020).

Figure 6.4 shows the values for the fit curves with the logistic function (Equation 6.3). Specific values are observed for each pair. For s over 350, all parameters show an almost constant evolution, behavior interpreted as an evolution of cross-correlations towards stability, at high values of the time scale of investigation. The parameter d has the largest variation for the pair CH_4 - temp, indicating the highest strength of multifractality. In the case of the analyzed data, the presence of a landfill serving the city of Bucharest, located in E-SE, not far from the observation area, could explain the presence and dynamics of the concentration CH_4 (Marin, C. A. et al., 2019b).

From the results of the investigations presented in these two subsections we can conclude the following:

- (i) nonlinear and multifractal characteristics exist both in the individual data series and in the case of cross-correlations in pairs;
- (ii) the highest strength of multifractality corresponds to ozone; (iii) all fluctuations are persistently correlated over the long term;
- (iv) for large fluctuations all correlations decrease to 0.5. We interpret this as proof that, while pollution accumulates in the short term, at longer intervals, it tends to a quasi-stationary state;
- (v) Generalized Hurst Exponent values are lower for cross-correlated datasets.

6.3 Analysis of the correlation of time series with atmospheric parameters in two types of urban environments

In this study we applied multifractal analysis for data series of PM_{10} , CO and temperature recorded in two different urban environments, traffic site (B6) and an urban background station (B1). It was chosen as the starting width of the time window $s \in (30, 150)$, corresponding to the interval (1.25 days, 6.25 days), with a step of 1 point. Then the window is moved and extended until it reaches the final width $s \in (40, 200)$ corresponding to the time interval of approximately (1.6 days, 8.33 days).

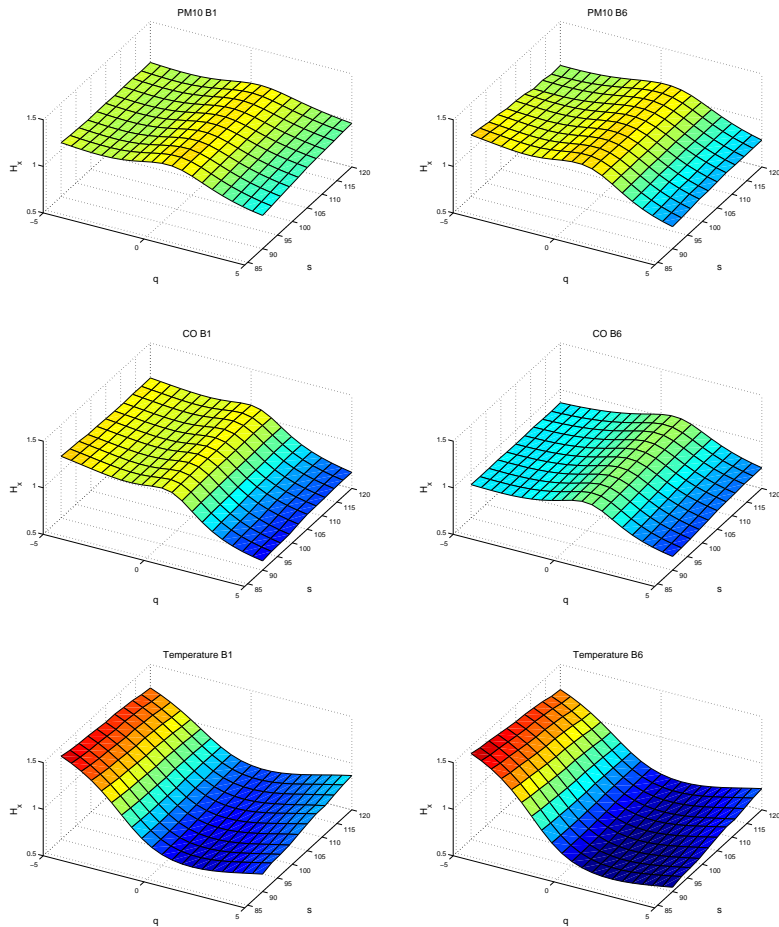


Figure 6.5: *Hurst surfaces for PM_{10} (first row), CO (second row) and temperature (third row) in the suburbs (station B1, left) and traffic (station B6, right)). (Marin, C.A. et al., 2021)*

The individual Hurst surfaces for PM_{10} , CO and the corresponding temperatures for the two averages are given in Figure 6.5. Analyzing the figure on the columns, we notice a change in the characteristics, with an increasing distance of horizontality, in the specific order PM_{10} , CO and temperature. This is equivalent to an increase in multifractality, which in turn is an indicator of the stability of

dynamics at different scales and fluctuation orders. Consequently, the most active dynamics are those involved in temperature variation. Followed by the data set of CO and PM₁₀ - which seems to have a more stable behavior. Analyzing by the type of the environment, the Hurst areas of the two stations are similar, with slightly lower values for the traffic station. For CO at low fluctuations, the urban site has higher values for H than the traffic site, while in the area of high fluctuations, the values of H decrease to approximately the same value. The strength of multifractality is higher for all parameters under the conditions of traffic, explainable by the more complex processes that take place in these locations, there are several sources to produce aerosols and gases which consequently causes complex chemical and physical reactions. For the case of CO, a different and quite similar dynamics is observed at large and small fluctuations, thus this data set less multifractal.

It was observed that the strength of multifractality is higher for the lowest analyzed scale (around 1 day) for all time series cross-correlated and decreases to the maximum scale (around 8 days). As a result, the strongest interactions occur on a small time scale. The strength of the multifractality is higher for the pair PM₁₀ - CO than for the temperature - PM₁₀ only at station B1, and the variation of the cross-correlation is large for the temperature pair - PM₁₀ at both stations. For comparison with urban measurements, we used CO data measured at a regional background site, E3 station, Poiana Stampei, located at an altitude of 900 m. Hurst surfaces for correlated sets of CO measured urban - regional indicates higher values at small fluctuations.

The analysis of the source of correlation present in the analyzed series was done through the procedure of mixing the data order. Prior to the random data rearrangement procedure, the surface has multifractality characteristics and long-term correlations. After mixing, the values for each independent series (H_X , H_Y) and for the correlated one (H_{XY}) approach 0.5, specifically a Gaussian noise. As a result, the source of multifractality is determined by long-type correlations for small and large fluctuations, on the whole time scale analyzed.

Final Conclusions

The doctoral thesis contributes with original data, analyzes and investigations to increase knowledge on the evolution of certain atmospheric chemical compounds (gases and aerosols) in the Magurele area, Bucharest, to identify sources and their origin, to study the formation of aerosols under experimental conditions and to highlight non-linear correlations between data series.

The thesis is structured in seven chapters. An introductory chapter (**Chapter 1**) that motivates the need for the study, purpose and objectives is followed by a brief presentation (**Chapter 2**) of the general techniques and instrumentation used to measure the physical and chemical properties of the atmospheric compounds. The following four chapters present original research in which the author has directly participated and whose results have been disseminated, as lead author or co-author, at national or international conferences or have been published in international journals with international impact. The studies and researches within the thesis pursue the four proposed objectives, as follows:

O1 assessment of gaseous constituents and aerosols concentrations in the cold season (Chapters 2 - 3)

This objective has been achieved by carrying out planned measurements and analyzes at national or international level. Participation in the internal campaign carried out between December 2017 and March 2018, together with 24 other European countries (with 57 measurement sites), facilitated measurements using a common working protocol, which allowed the harmonization of the recorded parameters at European level and ensured the quality of the data obtained.

The concentrations of the following gases : NO, NO₂, NO_x, O₃, CO, CH₄, SO₂ (in Chapter 2) and aerosols: PM₁, PM_{2.5}, PM₁₀, BC, OC, levoglucosan (in Chapter 3) were analyzed in terms of daytime dynamics, current regulations for **air quality** and links with meteorological parameters. For the cold season, the main polluting chemical compounds for Magurele were highlighted:

- Ozone exceeded the european limit (60 ppb) in two days of measurements, which implicitly led to decreases in concentrations of NO_x due to the links in the formation/destruction processes between the two pollutants. The other gases analyzed (NO₂, CO, SO₂) had average concentrations at least half of the European standards. According to the new rules recommended by the World Health Organization for particulate pollution with PM_{2.5}, in the measurement area there was a prolonged exposure (92 consecutive days) to concentrations considered toxic. For PM₁₀, several episodes of pollution were recorded, with the average daily value being exceeded in 28 of the 92 days of measurements.
- The concentrations of carbon compounds: OC, EC were among the highest

values recorded compared to the other 57 measurement sites in the 24 countries.

- Given **diurnal trends** the maximum pollutant concentrations are recorded in the morning and in the evening for the gases NO_x , CO, CH_4 and for aerosols PM_1 , PM_{10} . These maxima are influenced by local sources determined by anthropogenic activities, PBL altitude variation and meteorological conditions. For O_3 , CH_4 and CO, the dominant chemical and photochemical reactions influencing the change in the concentrations of these pollutants were highlighted.
- **Weekly Gas Trends** highlighted the highest concentrations of NO_x and SO_2 on Friday, when accumulation of pollutants emitted during the week occurred, as well as the intensification of other activities such as urban mobility. The smallest concentrations were registered on Sunday, which corresponds to reduced activities inside the urban agglomerations.

The importance of the study is given by the combined, continuous and long-term assessment of the simultaneous evolution of gas and particle concentrations during the cold season. This is the season in which there are several sources that can influence the concentrations of atmospheric constituents and it can have an effect on air quality and thus on human health through prolonged exposure to high levels of pollutants. Local monitoring and analysis of the evolution of pollutants is necessary to determine the episodes of pollution, and long-term studies show trends in the variation of pollutants and the effects of possible actions to stop pollution. In addition to the need for local monitoring and analysis of the evolution of pollutants, studies are also needed and required internationally for global analyses of transboundary air pollution.

O₂ estimation of contributing areas, local sources and long-distance transport for pollutants (Chapters 2 - 3 - 4).

To achieve this goal we used mathematical models such as NWR and PMF, but also physico-chemical measurements for desert dust aerosol. The studies present a differentiated assessment of gases and polluting particles sources, for the first time in the area of Bucharest by the spatial representation of their concentrations. For gases, the sources were estimated by the non-parametric regression method of the wind, obtaining:

- The main source of pollution with NO_x in the measurement area has been identified as the ring road of Bucharest with **traffic** associated with the transit of the area.
- During the cold season **residential heating** is one of the main sources and is observed from CO measurements, the emission points being distributed in the residential area close to the measuring area.
- Another source at a distance of approx. 8 km is a **landfill** that serves the city of Bucharest, identified only by measurements of CH_4 .
- **Remote anthropogenic / industrial sources** were identified using SO_2 as a marker.

For organic aerosols, determined by mass spectrometry, the contribution of the sources to the submicronic aerosol was estimated by the PMF method, observing:

- The main contributions to organic aerosols are given by the component **oxidized aerosols** (SOA) of two types OOA and OOA₂ - BBOA.
- A contribution of primary organic aerosol given by aerosols resulting from **traffic** (HOA).
- Another source of primary aerosols, **biomass burning** (BBOA), with a similar contribution to traffic.

A special type of **natural source**, type **desert dust**, was analyzed in a rare event of dust and snow deposition, from March 22-23, 2018 (Chapter 4). The problem of snow contamination was approached starting from the observed effect towards the generating cause. For the characterization of the aerosol, direct measurements and results obtained with remote sensing techniques were used in synergy together with complementary analyzes as follows:

- Satellite images show a cyclonic formation in Libya that started raising dust and transporting it to Europe. Wet deposition was the main phenomenon in removing desert dust from the atmosphere.
- In order to identify the type and source of the aerosol, snow samples were taken with embedded desert dust for which physical and chemical measurements were performed. These demonstrated the presence of specific elements **desert dust**, and reports of element concentrations identified the origin of the dust as **Northern Sahara**.
- Contaminations have been identified: before long-distance transport, due to the presence of biological markers (diatoms) specific to the South Saharan region, and during transport due to the presence of HULIS aerosols, specific to marine aerosol.

Measuring and analyzing pollutant variations to identify pollution episodes (activities at **O1**) is a topic of interest, but more important is solving the opposite problem, that of identifying the causes and sources of pollution (**O2**).

The quality of life in a given region is directly influenced by pollution and its chemical composition. The sources and their contribution bring us absolutely necessary information for adapting the pollution control strategies, by implementing measures aimed at the most contributing activities. The source evaluation studies in the analyzed area are of great scientific and community interest. Through the analyzes presented in this thesis and the reported publications (Section 8), the author contributed to the scientific documentation, for the first time, of the sources in the Bucharest-Magurele region. Understanding the episodes of pollution, knowing the sources, by identifying the amount of pollutants emitted from different activities (the results obtained at **O1** and **O2**) are necessary information for the decision makers, some of the results of these studies being disseminated in this purpose to the local and central authorities responsible for implementing pollution control strategies.

O3 investigating the formation of secondary aerosols using the oxidation chamber as an experimental technique

This objective is met in **Chapter 6**, which proposes an experimental configuration centered on an oxidation chamber, put into operation and calibrated for studies on the controlled formation of **secondary aerosols** with or without the addition of nucleation.

As there are few studies on the aging of environmental aerosols using the oxidation chamber, but also due to the dependence on local conditions, a series of tests have been made to establish the optimal assembly and parameters. The calibration of the oxidation chamber was done with sulfur dioxide, and the determined OH radical concentrations correspond to oxidation times (equivalent to normal environmental conditions) between 9 and 19 days. The measurements were scheduled for sequences of at least 24 hours, consisting of cycles alternating the voltage applied to the lamps between 0 and 3 V at equal time intervals.

By testing under different experimental conditions and case studies, the following were observed:

- When using a nucleating agent, SO₂, there is an increase in particle size of up to 90 nm, twice than the case with only ambient air oxidation
- In the case of the oxidation of atmospheric sample in the cold season, there was an **increase in organic secondary aerosol** and sulfate aerosol. Thus the oxidative conditions in the environment influence the mass concentration of the particles.
- For too oxidizing experimental conditions a possible **fragmentation** of the aerosol chain and a reduction of the mass concentration was observed.

The novelty of the study corresponding to the objective **O3**, is given by the realization of an experimental assembly involving the oxidation chamber, the first of its kind in Romania, necessary for detailed measurements on the formation of secondary aerosols. SOA is preponderant in the atmosphere, and its formation depends on many processes and reactions between precursors and other atmospheric constituents. Because oxidized organic compounds represent the major fraction of all organic aerosols, knowledge of sources and oxidation is required to estimate their lifetime, fragmentation, and thus their toxicity, which is interconnected with benzene nuclei present in polyaromatic compounds. In this context, the author contributes with important investigations and results related to the formation of SOA from environmental measurements. Through the studies started in this thesis, it was highlighted the particularity of the analysed site, given by the local sources, dependent on the season and the way in which the oxidative environmental conditions lead to the increase / decrease of PM concentrations.

O4 non-linear multifractal analysis of correlations between gases, aerosols and meteorological parameters

This objective is met in **Chapter 7**, which includes three separate cross-correlation studies between gases, aerosols, and meteorological parameters. The analyzes are based on the multifractal formalism, in the variant of the curves ($H(q)$) or of the representations of the surfaces of the generalized Hurst coefficients ($H(q, s)$).

The data are standardized and analyzed at the level of fluctuations, after the elimination of local trends. The behavior is described according to the size of the fluctuation, q , and the analysis time scale, s , through the formalism known in the literature as MM-DCCA, implemented by the author in Matlab. By comparing the value $H = 0.5$ specific to Gaussian noise, persistent or non-persistent correlations can be determined for the following cases:

- Correlations between particle concentration (with dimensions between 0.5 and 20 μm), their size and meteorological parameters (air temperature, wind speed, solar radiation, relative humidity and pressure).

An anticorrelation was observed between particle concentration and meteorological parameters and a long-term correlation for the pairing between particle size and humidity. Also, the strength of the correlations between the weather conditions and the total average concentration is higher than between the weather conditions and the average diameter of the aerosols.

- Cross-correlations between ozone and its precursors: NO_x , CH_4 , NMHC, THC, and temperature.

All individual data as well as cross-linked data series have multifractal properties and long-term persistent correlations. New parameters have been proposed to differentiate Hurst surfaces: the strength of multifractality and the variation of cross-correlation. The highest values were found for ozone, which confirms the existence of a large number of variables that affect its dynamics. By evaluating the parameters of the logistic curves, proposed as fitting functions for Hurst exponents, specific characteristics of each data pair were found. At high values of the analysis scale (s), the fitting parameters show an almost constant evolution which indicates a long-term cross-correlation stability. The parameter defined for estimating the global correlation ($\eta_{s(XY)}(q)$) provides information about both the cross-correlation for the entire time scale and the individual contribution of each data set in a given combination. The data pair $O_3 - NO_x$ was confirmed to be the most dynamic pair, strongly connected due to the chemical reactions between them, and the multifractality of the data ozone has a dominant influence on the data pairs analyzed.

- Simple and cross-correlations for PM_{10} , CO and temperature, for three different types of locations: city-background, city-traffic, and regional.

Experimental recordings for these atmospheric parameters showed long-term correlated fluctuations. The data series PM_{10} has a stable dynamic, and the strength of the multifractality is higher for the pair PM_{10} - temperature in the traffic station, comparative with the urban background. Applying a random data mixing process, it was found that the source of multifractality is given by long-term correlations.

Compared to traditional methods, this analysis has significant advantages, by exploring the real atmospheric system at different time scales, without any initial hypothesis on the complex mechanisms of interaction between atmospheric constituents. The proposed analysis quantitatively describes the essential characteristics

of short-term and long-term dynamics, reveals the type of dynamics (deterministic or stochastic) and quantifies its complexity. The multifractal analysis method highlights the specific time scales and, for different pairs of data sets, reveals the contribution of each individual data set to the corresponding cross-series, for both small and large fluctuations.

The results of the studies presented in this paper were published in **eight** scientific papers published in listed journals **ISI**, an ISI proceeding and were reported at eight international conferences (**four** oral presentations and **four** posters).

Future directions

The studies presented for the characterization of gaseous constituents and pollutants during the cold season at the site in Magurele, may be continued with future investigations to describe diurnal trends and chemical reactions and during the hot season when photooxidation processes are more important. In addition, estimating sources in other seasons would be of particular interest for highlighting the influence of other seasonal or accidental activities and sources. and possible new correlations. Air quality, an important issue in Romania, should be investigated for as long as possible and also in different types of locations (urban, regional and background). Multiannual statistics may show the effect of national legislation on pollutant emission rates and whether further action is needed to meet the recommendations of the European Union or the World Health Organization. It is also important to assess sources in several cities with environmental problems, and a combined analysis of atmospheric constituent data with morbidity/mortality data is needed to assess the impact on human health. For example, in Romania there are no studies on the impact of fine and ultrafine particles on health, so the data presented in the thesis can be associated and correlated with medical information and statistics.

SOA formation case studies and analysis protocol can be used in future investigations to understand the formation of secondary aerosols when different types of primary aerosols are present in the atmosphere (waste burning, vegetation fires). An important step would be to obtain from the measurements made in the reaction chamber specific SOA characteristics (such as spectral fingerprints, optical parameters) which could be used later in the source estimation processes. Another study of interest is the determination of the effect of SOA on the formation of cloud condensation nuclei.

Given the complex dynamics of the atmosphere, multifractal analyzes can be applied in future studies not only on pair variables, but on cross-sectional data sets such as concentration data and climatological data. Due to the impact of atmospheric constraints on health, nonlinear analyzes of multifractal correlations can be used to highlight hidden interdependencies between polluting atmospheric parameters and health data.

Selective Bibliography

- Adame, J., Notario, A., Villanueva, F., și Albaladejo, J. (2012). Application of cluster analysis to surface ozone, NO₂ and SO₂ daily patterns in an industrial area in Central-Southern Spain measured with a DOAS system. *Science of The Total Environment*, 429:281–291. Special Section - Arsenic in Latin America, An Unrevealed Continent: Occurrence, Health Effects and Mitigation.
- Ahlberg, E., Ausmeel, S., Eriksson, A., Holst, T., Karlsson, T., Brune, W., Frank, G., Roldin, P., Kristensson, A., și Svenningsson, B. (2019). No Particle Mass Enhancement from Induced Atmospheric Ageing at a Rural Site in Northern Europe. *Atmosphere*, 10:408.
- Anderson, J. O., Thundiyil, J. G., și Stolbach, A. (2012). Clearing the air: A review of the effects of particulate matter air pollution on human health. *Journal of Medical Toxicology*, 8:66—175.
- Andrews, E., Sheridan, P. J., Fiebig, M., McComiskey, A., Ogren, J. A., Arnott, P., Covert, D., Elleman, R., Gasparini, R., Collins, D., Jonsson, H., Schmid, B., și Wang, J. (2006). Comparison of methods for deriving aerosol asymmetry parameter. *J. Geophys. Res.*, 111:D05S04.
- Crippa, M., Canonaco, F., Lanz, V. A., Äijälä, M., Allan, J. D., Carbone, S., Capes, G., Ceburnis, D., Dall’Osto, M., Day, D. A., DeCarlo, P. F., Ehn, M., Eriksson, A., Freney, E., Hildebrandt Ruiz, L., Hillamo, R., Jimenez, J. L., Junninen, H., Kiendler-Scharr, A., Kortelainen, A.-M., Kulmala, M., Laaksonen, A., Mensah, A. A., Mohr, C., Nemitz, E., O’Dowd, C., Ovadnevaite, J., Pandis, S. N., Petäjä, T., Poulain, L., Saarikoski, S., Sellegri, K., Swietlicki, E., Tiitta, P., Worsnop, D. R., Baltensperger, U., și Prévôt, A. S. H. (2014). Organic aerosol components derived from 25 AMS data sets across Europe using a consistent ME-2 based source apportionment approach. *Atmospheric Chemistry and Physics*, 14(12):6159–6176.
- Crippa, M., DeCarlo, P. F., Slowik, J. G., Mohr, C., Heringa, M. F., Chirico, R., Poulain, L., Freutel, F., Sciare, J., Cozic, J., Di Marco, C. F., Elsasser, M., Nicolas, J. B., Marchand, N., Abidi, E., Wiedensohler, A., Drewnick, F., Schneider, J., Borrmann, S., Nemitz, E., Zimmermann, R., Jaffrezo, J.-L., Prévôt, A. S. H., și Baltensperger, U. (2013). Wintertime aerosol chemical composition and source apportionment of the organic fraction in the metropolitan area of Paris. *Atmospheric Chemistry and Physics*, 13(2):961–981.
- Donateo, A., Feudo, T. L., Marinoni, A., Dinoi, A., Avolio, E., Merico, E., Calidonna, C., Contini, D., și Bonasoni, P. (2018). Characterization of in situ aerosol

- optical properties at three observatories in the central mediterranean. *Atmosphere*, 9:369.
- Ealo, M., Alastuey, A., Ripoll, A., Pérez, N., Minguillón, M., Querol, X., și Pandolfi, M. (2016). Detection of Saharan dust and biomass burning events using near-real-time intensive aerosol optical properties in the north-western Mediterranean. *Atmos. Chem. Phys.*, 16:12567–12586.
- Gurjar, B., Jain, A., Sharma, A., Agarwal, A., Gupta, P., Nagpure, A., și Lelieveld, J. (2010). Human health risks in megacities due to air pollution. *Atmospheric Environment*, 44(36):4606–4613.
- Hallar, A. G., Petersen, R., Andrews, E., Michalsky, J., McCubbin, I. B., și Ogren, J. A. (2015). Contributions of dust and biomass burning to aerosols at a Colorado mountain-top site. *Atmos. Chem. Phys.*, 15:13665–13679.
- IPCC, Masson–Delmotte, V., Zhai, P., Pirani, A., Connors, S. L., Péan, C., Berger, S., Caud, N., Chen, Y., Goldfarb, L., Gomis, M. I., Huang, M., Leitzell, K., Lonnoy, E., Matthews, J. B. R., Maycock, T. K., Waterfield, T., Yelekçi, O., Yu, R., și Zhou, B. (2021a). *Climate Change 2021: The Physical Science Basis. Contribution of Working Group I to the Sixth Assessment Report of the Intergovernmental Panel on Climate Change*. Cambridge University Press, In Press.
- IPCC, Masson–Delmotte, V., Zhai, P., Pirani, A., Connors, S. L., Péan, C., Berger, S., Caud, N., Chen, Y., Goldfarb, L., Gomis, M. I., Huang, M., Leitzell, K., Lonnoy, E., Matthews, J. B. R., Maycock, T. K., Waterfield, T., Yelekçi, O., Yu, R., și Zhou, B. (2021b). *Summary for Policymakers in Climate Change 2021: The Physical Science Basis. Contribution of Working Group I to the Sixth Assessment Report of the Intergovernmental Panel on Climate Change*. Cambridge University Press, In Press.
- Jimenez, J. L., Canagaratna, M. R., Donahue, N. M., Prevot, A. S. H., Zhang, Q., Kroll, J. H., DeCarlo, P. F., Allan, J. D., Coe, H., Ng, N. L., Aiken, A. C., Docherty, K. S., Ulbrich, I. M., Grieshop, A. P., Robinson, A. L., Duplissy, J., Smith, J. D., Wilson, K. R., Lanz, V. A., Hueglin, C., Sun, Y. L., Tian, J., Laaksonen, A., Raatikainen, T., Rautiainen, J., Vaattovaara, P., Ehn, M., Kulmala, M., Tomlinson, J. M., Collins, D. R., Cubison, M. J., Dunlea, E. J., Huffman, J. A., Onasch, T. B., Alfarra, M. R., Williams, P. I., Bower, K., Kondo, Y., Schneider, J., Drewnick, F., Borrmann, S., Weimer, S., Demerjian, K., Salcedo, D., Cottrell, L., Griffin, R., Takami, A., Miyoshi, T., Hatakeyama, S., Shimono, A., Sun, J. Y., Zhang, Y. M., Dzepina, K., Kimmel, J. R., Sueper, D., Jayne, J. T., Herndon, S. C., Trimborn, A. M., Williams, L. R., Wood, E. C., Middlebrook, A. M., Kolb, C. E., Baltensperger, U., și Worsnop, D. R. (2009). Evolution of Organic Aerosols in the Atmosphere. *Science*, 326:1525–1529.
- Lafon, S., Sokolik, I. N., Rajot, J. L., Caquineau, S., și Gaudichet, A. (2006). Characterization of iron oxides in mineral dust aerosols: Implications for light absorption. *J. Geophys. Res.*, 111:D21207.

- Manousakas, M., Florou, K., și Pandis, S. (2020). Source Apportionment of Fine Organic and Inorganic Atmospheric Aerosol in an Urban Background Area in Greece. *Atmosphere*, 11:330.
- Marmureanu, L., **Marin, C. A.**, Vasilescu, J., și Antonescu, B. (2019). Preliminary results of winter intensive campaign ACTRIS-COLOSSAL in Romania, Comunicare orală prezentată la întâlnirea Colossal, 2019, Spania.
- Moosmüller, H., Engelbrecht, J. P., Skiba, M., Frey, G., Chakrabarty, R. K., și Arnott, W. P. (2012). Single scattering albedo of fine mineral dust aerosols controlled by iron concentration. *J. Geophys. Res.*, 117:D11210.
- Müller, D., Ansmann, A., Freudenthaler, V., Kandler, K., Toledano, C., Hiebsch, A., Gasteiger, J., Esselborn, M., Tesche, M., Heese, B., Althausen, D., Weinzierl, B., Petzold, A., și von Hoyningen-Huene, W. (2010). Mineral dust observed with AERONET Sun photometer, Raman lidar, and in situ instruments during SAMUM 2006: Shape-dependent particle properties. *J. Geophys. Res.*, 115:D11207.
- Mărmureanu, L., **Marin, C.A.**, Andrei, S., Antonescu, B., Ene, D., Boldeanu, M., Vasilescu, J., Vițelaru, C., Cadar, O., și Levei, E. (2019). Orange Snow—A Saharan Dust Intrusion over Romania During Winter Conditions. *Remote Sens.*, 11:2466.
- Mărmureanu, L., Vasilescu, J., Slowik, J., Prévôt, A. S. H., **Marin, Cristina Antonia**, Antonescu, B., Vlachou, A., Nemuc, A., Dandocsi, A., și Szidat, S. (2020). Online Chemical Characterization and Source Identification of Summer and Winter Aerosols in Măgurele, Romania. *Atmosphere*, 11(4).
- Ogren, J. A., Andrews, E., McComiskey, A., Sheridan, P., Jefferson, A., și Fiebig, M. (2006). New insights into aerosol asymmetry parameter. *Proceedings of the 16th ARM Science Team Meeting*.
- Petit, J.-E., Favez, O., Albinet, A., și Canonaco, F. (2017). A user-friendly tool for comprehensive evaluation of the geographical origins of atmospheric pollution: Wind and trajectory analyses. *Environmental Modelling & Software*, 88:183–187.
- Pfeifer, S., Müller, T., Weinhold, K., Zikova, N., dos Santos, S. M., Marinoni, A., Bischof, O. F., Kykal, C., Ries, L., Meinhardt, F., Aalto, P., Mihalopoulos, N., și Wiedensohler, A. (2016). Intercomparison of 15 aerodynamic particle size spectrometers (APS 3321): uncertainties in particle sizing and number size distribution. *Atmos. Meas. Tech.*, 9:1545–1551.
- Platt, S. (2019). Results from EMEP/COLOSSAL/ACRTIS intensive measurement campaign, Comunicare orală prezentată la întâlnirea Colossal, 2019, Spania.
- Scheuven, D., Schütz, L., Kandler, K., Ebert, M., și Weinbruch, S. (2013). Bulk composition of northern African dust and its source sediments — A compilation. *Earth. Sci. Rev.*, 16:170–194.
- Sillman, S. (1999). The relation between ozone, nox and hydrocarbons in urban and polluted rural environments. *Atmospheric Environment*, 33(12):1821–1845.

- Stan, C., Balasoiu, M., Buzatu, D., și Cristescu, C. (2017). Multifractal analysis of coFe₂O₄/lauric acid/DDS-Na/H₂O ferrofluid from transmission electron microscopy measurements. *Journal of Computational and Theoretical Nanoscience*, 14:2030–2034.
- Stan, C., Marmureanu, L., **Cristina Marin**, și Cristescu, C. P. (2020). Investigation of multifractal cross-correlation surfaces of Hurst exponents for some atmospheric pollutants. *Physica A: Statistical Mechanics and its Applications*, 545:123799.
- Telloli, C., Chicca, M., Pepi, S., și Vaccaro, C. (2018). Saharan dust particles in snow samples of Alps and Apennines during an exceptional event of transboundary air pollution. *Environ. Monit. Assess.*, 190:37.
- Marin, C.**, Stan, C., Preda, L., Marmureanu, L., Belegante, L., și Cristescu, C. (2018). Multifractal cross correlation analysis between aerosols and meteorological data. *Rom. J. Phys.*, 63:805.
- Marin, C. A.**, Marmureanu, L., Dandocsi, A., Antonescu, B., Andrei, S., Radu, C., și Stan, C. (2019a). Winter intensive measurement campaign at Magurele, Romania, poster prezentat la conferința European Aerosol Conference, EAC 2019, Suedia.
- Marin, C. A.**, Mărmureanu, L., Radu, C., Dandocsi, A., Stan, C., Țoancă, F., Preda, L., și Antonescu, B. (2019b). Wintertime Variations of Gaseous Atmospheric Constituents in Bucharest Peri-Urban Area. *Atmosphere*, 10(8).
- Marin, C.A.**, Stan, C., și Cristescu, C. (2021). Multifractal cross-correlation of atmospheric pollutants and temperature in different environments. *U.P.B. Sci. Bull., Series A*, 83:227–238.

List of contributions

8.1 Published Papers

8.1.1 ISI Papers

1. Marmureanu, L., Vasilescu, J., **Marin, C.**, Ene, D. (2017) Aerosol Source Assessment Based on Organic Chemical Markers, *Revista de Chimie*, 68(4), pp. 853-857, **AIS=0.047, IF=1.412**;
2. **Marin, C.**, Stan, C., Preda, L., Marmureanu, L., Belegante, L., Cristescu, C. P., (2018) Multifractal Cross Correlation Analysis between Aerosols and Meteorological Data, *Romanian Journal of Physics* 63, 805, **AIS=0.208, IF=1.46**;
3. **Marin, C.A.**, Marmureanu, L., Radu, C., Dandocsi, A., Stan, C., Toanca, F., Preda, L., Antonescu, B., (2019) Wintertime Variations of Gaseous Atmospheric Constituents in Bucharest Peri-Urban Area, *Atmosphere*, 10, 478, **AIS=0.549, IF=2.397**;
4. Marmureanu, L., **Marin, C. A.**, Andrei, S., Antonescu, B., Ene, D., Boldeanu, M., Vasilescu, J., Vitelaru, C., Cadar, O., Levei, E., (2019) Orange Snow-A Saharan Dust Intrusion over Romania During Winter Conditions, *Remote Sensing*, 11, 2466, **AIS=0.929, IF=4.509**;
5. Stan, C., Marmureanu, L., **Marin, C.**, Cristescu, C. P., (2020) Investigation of multifractal cross-correlation surfaces of Hurst exponents for some atmospheric pollutants, *Physica A-Statistical Mechanics And Its Applications*, 545, 123799, **AIS=0.511, IF=3.263**;
6. Marmureanu, L., Vasilescu, J., Slowik, J., Prevot, A.S.H., **Marin, C. A.**, et al. (2020) Online Chemical Characterization and Source Identification of Summer and Winter Aerosols in Magurele, Romania, *Atmosphere*, 11, 385, **AIS=0.626, IF=2.686**;
7. **Marin, C.**, Stan, C., Cristescu, C. P., (2021) Multifractal cross-correlation of atmospheric pollutants and temperature in different environments, *University Politehnica Of Bucharest Scientific Bulletin-Series A-Applied Mathematics And Physics*, 83, 227-238, **AIS=0.16, IF=0.903**;
8. Chen, G., **Marin, C.**, et al (2022) European Aerosol Phenomenology – 8: Harmonised Source Apportionment of Organic Aerosol using 22 Year-long ACSM/AMS Datasets, *Environment International*, **AIS=2.122, IF=9.621**

Total AIS= 5.152 ; Total IF=26.251

8.1.2 Additional ISI Papers

1. Dandocsi, A., Marmureanu, L., **Marin, C.**, Puscas, N., (2019) Comparison Of Carbon Monoxide Data Products From Sentinel-5 precursor With Low Resolution FTIR Spectrometer, University Politehnica Of Bucharest Scientific Bulletin-Series A-Applied Mathematics And Physics, 81, 201-214, AIS=0.086, IF=0.619;
2. Andrei, S., Antonescu, B., Boldeanu, M., Marmureanu, L., **Marin, C. A.**, Vasilescu, J., Ene, D., (2019) An Exceptional Case of Freezing Rain in Bucharest (Romania), Atmosphere, 10, 673, AIS=0.549, IF=2.397;
3. Antonescu, B., Mărmureanu, L., Vasilescu, J., **Marin, C.**, Andrei, S., Boldeanu, M., Ene, D., Țilea, A. (2021) A 41-year bioclimatology of thermal stress in Europe. Int J Climatol.; 41: 3934– 3952. <https://doi.org/10.1002/joc.7051>, AIS=1.271, IF=4.069

8.1.3 ISI indexed papers

1. **Marin C.**, Vasilescu, J., Marmureanu, L., Ene, D., Preda, L., Mihailescu, M., (2018) Biomass burning aerosols characterization from ground based and profiling measurements, EPJ Web of Conferences, 176, 08013

8.2 International conference contributions

1. **Marin, C.**, Dandocsi, A., Radu, C., Marmureanu, L., and C. Stan, Gas concentration variations and source assessment during winter in Magurele, Romania, THE 6th International Colloquim “Physics Of Materials” (PM 6), Bucharest, Romania, 2018 (**comunicare orală**);
2. **Marin, C.**, Marmureanu, L., Andrei, S., Antonescu, B., Boldeanu, M., Vasilescu, J., Dandocsi, A., Biomass burning emissions- multianul statistics in Romania, International Conference Environment at a Crossroads: SMART approaches for a sustainable future- EcoSmart, Bucharest, Romania, 2019 (**comunicare orală**);
3. **Marin, C.**, Marmureanu, L., Andrei, S., Antonescu, B., Ene, D., Boldeanu, M., Vasilescu, J., Vitelaru, C., Cadar, O., Levei, E., A Major Saharan Dust Intrusion Over Romania, WeBIOPATR19, Belgrad, Serbia, 2019 (**comunicare orală**);
4. **Marin, C.**, et al, Overview of the WASTE project and Romanian contribution, Science for Environment and Climate in Romania, Bucuresti,2021 (**comunicare orală**);
5. **Marin, C.**, Noblet, C., Amodeo,T., Aujay-Plouzeau,R., Karoski, N., Lestremau, F., Petit, J.-E., Truong, F., Besombes,J.-L., Favez, O., Gros, V., Marmureanu,L., Albinet, A., A preliminary study of real-time measurements of secondary organic aerosol (SOA) formation and aging from ambient air in a potential aerosol mass reactor (PAM) in the Paris area, ELSEDIMA, Cluj-Napoca, Romania, 2018 (poster)
6. **Marin, C. A.**, Marmureanu, L., Dandocsi, A., Antonescu, B., Andrei, S., Radu, C.,and Stan, C., Winter Intensive Measurement Campaign at Magurele, Romania, European Aerosol Conference, Suedia, 2019 (poster)

7. Marmureanu, L., Dandocsi, A., **Marin, C. A.**, Oikonomou, K., Sciare, J., Assessment of black carbon influences on air quality in a suburban area from eastern Europe during winter season, European Aerosol Conference, Suedia, 2019 (poster)
8. Vasilescu, J., Marmureanu, L., **Marin, C. A.**, Dandocsi, A., Multiannual seasonal analysis of submicron aerosol variability and organic fraction sources at Magurele site, European Aerosol Conference, Suedia, 2019 (poster)